Probing Vesicles Dynamics in Single Hippocampal Synapses

by

Matthew Shtrahman

BS in Biochemistry, University of Michigan, 1997

Submitted to the Graduate Faculty of

Arts and Sciences in partial fulfillment

of the requirements for the degree of

PhD in Physics and Astronomy

University of Pittsburgh

2005

UNIVERSITY OF PITTSBURGH

FACULTY OF ARTS AND SCIENCES

This dissertation was presented

by

Matthew Shtrahman

It was defended on

March 28, 2005

and approved by

Xiao-lun Wu, PhD Professor

Guo-qiang Bi, PhD Assistant Professor

David Jasnow, PhD Professor

Jeremy Levy, PhD Associate Professor

Steve Meriney, PhD Associate Professor

Dissertation Director: Xiao-lun Wu, PhD Professor

Copyright © by Matthew Shtrahman
2005

Probing Vesicle Dynamics in Single Hippocampal Synapses

Matthew Shtrahman, PhD

University of Pittsburgh, 2005

The classic mode of communication between neurons occurs via chemical synapses. In this process, vesicles dock at the active zone and fuse with the cell membrane, emptying neurotransmitter into the synaptic cleft. This process is stochastic and the efficacy of synaptic communication depends on the availability and movement of vesicles. We use fluorescence correlation spectroscopy (FCS) and fluorescence recovery after photobleaching (FRAP) to study vesicle dynamics inside the synapses of cultured hippocampal neurons labeled with the fluorescent vesicle marker FM 1-43. These studies show that when the cell is electrically at rest, only a small population of vesicles is mobile, taking seconds to traverse the synapse. Applying the phosphatase inhibitor okadaic acid (OA) causes vesicles to diffuse freely, moving 30 times faster than vesicles in control synapses. In contrast, eliminating polymerized synaptic actin does not free vesicles. These results suggest that vesicles move sluggishly due to binding to structural proteins within the synapse, and that this binding is altered by phosphorylation. Motivated by these results, a model is constructed consisting of diffusing vesicles that bind reversibly within the synapse. This stick-and-diffuse model accounts for the FCS and FRAP data, and also predicts the well-known exponential refilling of the readily releasable pool. Our measurements suggest that the movement of vesicles to the active zone is the rate limiting step in this process.

TABLE OF CONTENTS

LIST OF FIGURES

PREFACE

Physics is the study of natural phenomena. It is in this sense that the field of biology is an important discipline within physics, analogous to astronomy. There exists a long history of physicists that have worked in the area of biology, and have made significant contributions to the field. These include among others Howard Berg, Lawrence and William Bragg, Francis Crick, Max Delbruck, Edward Purcell, and Leo Szilard. The biology of the brain and the nervous system is not an exception. Traditionally, physicists' greatest contributions to experimental neurobiology occurred via the development of novel techniques to study previously unanswerable questions. The invention of the patch clamp (Neher and Sakmann 1976), nuclear magnetic resonance techniques (Bloch, Hanson et al. 1946; Purcell, Torrey et al. 1946), and two-photon fluorescence microscopy (Denk, Strickler et al. 1990) are notable examples that are widely used by experimentalists today, decades after their inception. While these technical achievements represent major contributions to experimental neuroscience, the role of the physicist in experimental neuroscience and biology is perceived as largely technical in nature. This attitude has not changed significantly since 1967 when the physicist Sergei Feitelberg proposed that the "spectacular developments (in biology) created a clear and unequivocal need for physicists and their help, the role of the physicist was that of a glorified technician engaged in methodology and instrumentation, dignified only by the strangeness of his doings and the mysteriousness of his tools" (Varmus 1999). I envision a time when physicists will shed this

perception and introduce revolutionary ideas and questions to the study of the brain that have the same impact as the technical achievements described above.

One may argue that the work presented in this thesis, like much contemporary work in biology, is highly focused in its scope and largely technical in its achievement. However, I hope that this work will stimulate the reader to ponder new questions about the brain, as it has done for the author.

I would like to acknowledge several people who contributed directly or indirectly to this work. David Nauen edited our journal manuscripts, which were incorporated into the thesis. Pakming Lau, Huaixing Wang, and Xi Zhao prepared the neuronal cultures used in the experiments. In addition, Xi Zhao prepared the neuronal culture transfected with GFP-actin. I am greatly indebted to Chuck Yeung who constructed the theoretical models described in the thesis and our collaborator, Guoqiang Bi who contributed many of the essential ideas presented in this work. Lastly, I would like to thank my advisor Xiao-lun Wu, who not only supported me financially and intellectually, but guided me through entire PhD process.

1. INTRODUCTION

1.1. OVERVIEW OF THE BRAIN

The human brain contains 10^{11} neurons (Lange 1975; Pakkenberg and Gundersen 1997), which are thought to be its computational units. The brain also contains glial cells, which according to some investigators outnumber neurons 10:1 (Stevens 2003). However, the extent of their role in computation is not entirely clear. Together, these cells are densely packed within the brain's modest volume of approximately 1350 cm^3 (Pakkenberg and Gundersen 1997). Neurons utilize the electrochemical potential across their membrane to code for information, discharging electrical spikes similar to a digital code (Rieke, Warland et al. 1998). Like other many body systems, the interactions between these units largely govern the dynamics of the system. Neurons within the brain are densely connected, with the average neuron making approximately 10^4 direct connections, or synapses (Pakkenberg and Gundersen 1997; Pakkenberg, Pelvig et al. 2003). Synapses are neuronal junctions with well defined structure that couple neurons via chemical signals. This coupling can be inhibitory or excitatory, and the strength of the interaction can be modulated on time scales of milliseconds to hours, and even longer (Abbott and Regehr 2004). It is thought that memory is the information stored in the spatial pattern of synaptic strengths within the brain, and that learning is the process of optimizing these interactions as the result of experience. Together memory and learning influence behavioral phenomena such as perception and cognition, which are hypothesized to be represented by distinct spatiotemporal patterns of neuronal excitation. Unfortunately, the global dynamics of

the brain, similar to most many body systems, is prohibitively complicated and difficult to study experimentally, and is beyond the scope of this work. The focus of this thesis is at the level of the synapse, and we devote the remainder of the introduction to the function of this cellular structure.

1.2. SYNAPTIC TRANSMISSION

Neurons, similar to other cells have an electrical potential across their outer membrane, where the inside of the neuron is about -70 mV with respect to the extracellular space. This voltage fluctuates in response to the injection of current from the synaptic transmission elicited by connecting neurons, which we discuss below. If the voltage exceeds a threshold (-40 to -50 mV), a population of voltage sensitive protein channels, embedded within the membrane, open and allow Na^+ ions to flow into the cell. This inflow is followed approximately a millisecond later by the outflow of K^+ ions, resulting in a narrow voltage spike called an action potential. These ions diffuse down existing concentration gradients, which are maintained by ion pumps that run continuously. The membrane containing the voltage sensitive channels mentioned above extends from the cell body or soma to an output cable called the axon, which propagates the action potential as a traveling wave (Fig 1). The axon bifurcates many times, with the terminus of each branch forming a synapse with a connecting postsynaptic cell. The terminus of the axon, called the synaptic bouton, is filled with 40 nm vesicles that are packed with small signaling molecules called neurotransmitters. The action potential arrives at the bouton and triggers a variety of events, the first of which is the influx of Ca^{2+} ions. These events culminate in the fusion of a vesicle's membrane with the outer membrane of the bouton, and the release of the neurotransmitter molecules into the extracellular space. This vesicle fusion and release of

neurotransmitter, called exocytosis, can only occur at a specialized section of the bouton's outer membrane. This region, known as the active zone, contains the proper protein machinery required for vesicles to dock or bind to specific release sites in the synaptic membrane and undergo membrane fusion. The membrane of the postsynaptic or connecting cell is directly opposed to the active zone, with a 20 nm gap between the two membranes. The neurotransmitter diffuses across this gap or synaptic cleft, where it binds to a variety of protein receptors embedded in the postsynaptic membrane. A subset of these receptors are channels, and upon binding to neurotransmitter they allow particular ions to flow in or out of the postsynaptic cell. The resulting post synaptic current (PSC) propagates along input cables called dendrites and towards the cell body of the postsynaptic cell. In the proximal axon, near the soma, the electrical contributions from many synapses are integrated in a linear fashion (Cash and Yuste 1998). If the resulting voltage reaches threshold, then the postsynaptic cell fires an action potential and the signal propagates along the axon to another set of synapses.

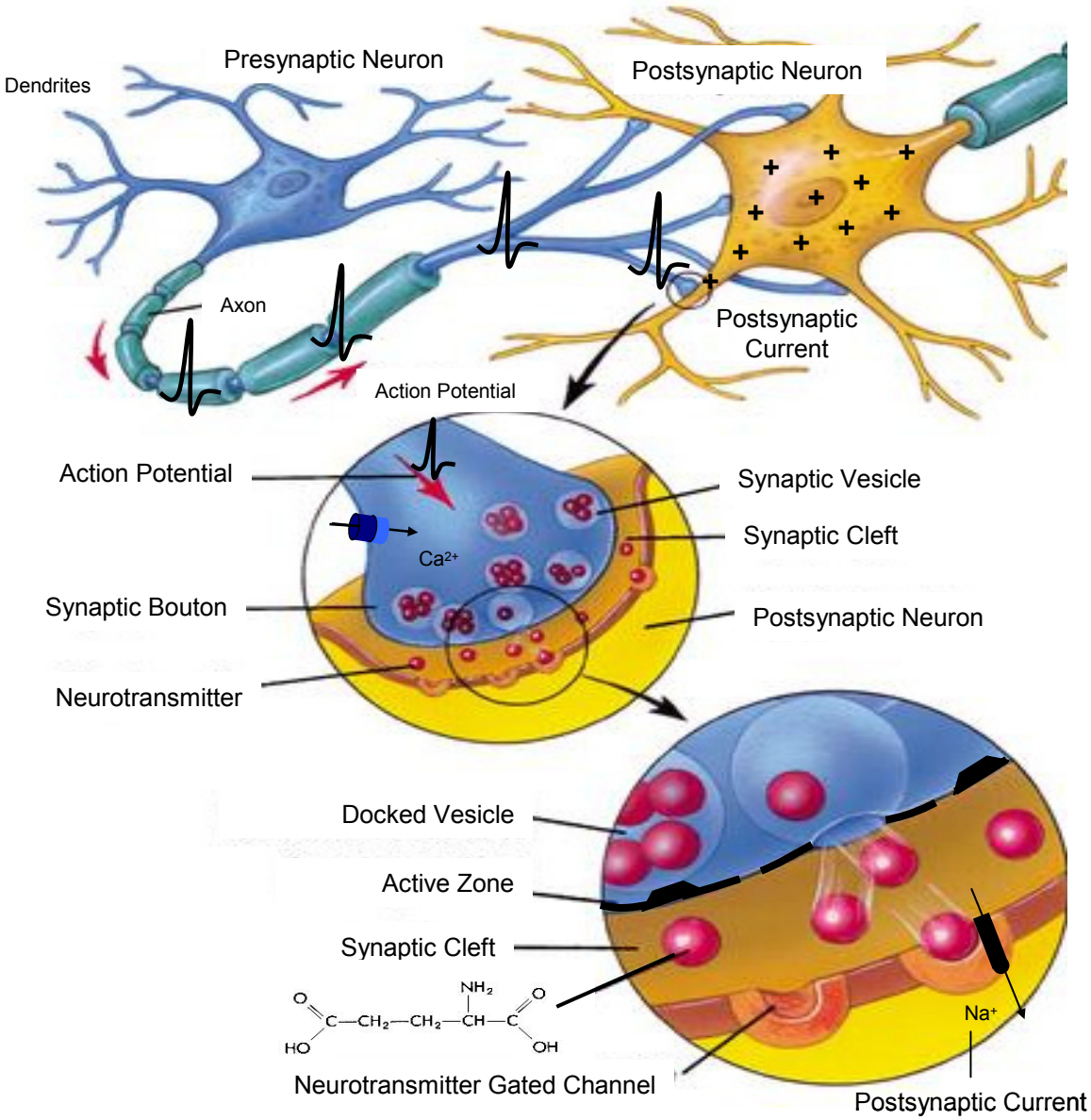

Figure 1 Excitatory Synaptic Transmission (unknown source)**.** An action potential travels along the axon of an excited presynaptic cell and enters the synaptic bouton, causing voltage gated Ca^{2+} channels to open. The influx of Ca^{2+} initiates a sequence of events that ultimately leads a docked vesicle to fuse with the plasma membrane, releasing the neurotransmitter glutamate into the synaptic cleft. Glutamate diffuses across the synaptic cleft and binds to glutamate receptors, which can lead to a variety of actions depending on the receptor subtype. One important consequence is the influx of Na^{+} ions into the cell, resulting in an excitatory post synaptic current (EPSC).

1.3. SYNAPTIC VESICLE CYCLE

As discussed above, vesicles in the bouton undergo exocytosis, where they fuse with the membrane of the presynaptic cell and empty their contents into the extracellular space. The cell replenishes the limited supply of vesicles by pinching off portions of the outer membrane through a process called endocytosis. These newly formed vesicles are then filled with neurotransmitter, travel to the active zone, dock, and prime before they are available to undergo exocytosis. Most of these processes happen in succession and form what is known as the synaptic vesicle cycle (Fig 2). The timescale to complete this cycle and the number of release competent vesicles in the bouton limit the steady state rate at which vesicles can exocytose. As we will discuss in the next section, there are less than 40 recycling vesicles in the type of synaptic boutons studied here, and the time to navigate the entire cycle is at least 40 seconds. Therefore, the steady state rate of exocytosis cannot exceed 1 Hz (Pyle, Kavalali et al. 2000). Hence, this cycle places severe restrictions on the dynamics of synaptic transmission between neurons and their resulting electrical activity.

Within the cycle, there exists another parallel pathway for vesicle recycling called rapid endocytosis or “kiss-and-run” (Fig 2). Here vesicles bypass several of the steps outlined above, increasing the rate at which vesicles become available for exocytosis. However, as we discuss in section 1.6, this appears to be a rare mode of vesicle recycling that does not alleviate the restrictions discussed above.

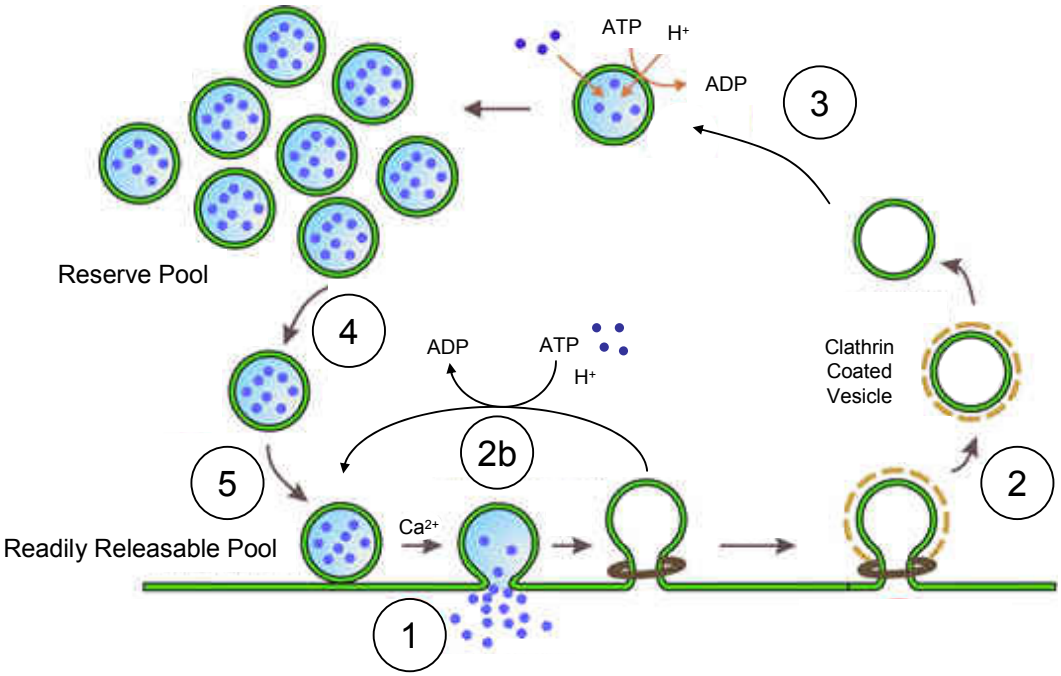

Figure 2 Synaptic Vesicle Cycle (Cousin 2005). 1. *Exocytosis*. Ca influx triggers the vesicular membrane to fuse with the neuron's plasma membrane, releasing neurotransmitter. 2. *Endocytosis*. Several proteins including clathrin assemble and induce the membrane to invaginate, forming a vesicle. 2b. *Kiss-and-run*. Alternatively, the vesicle membrane does not completely fuse and the vesicle remains docked. There it can be filled with neurotransmitter and primed for another exocytosis event. 3. *Neurotransmitter Transport*. The H^+-ATPase pumps H^+ ions into the vesicle interior or lumen. This results in an electrical potential and pH gradient that can be utilized to pump neurotransmitter molecules into the vesicle. 4. *Vesicle Movement*. Recycling vesicles must move from distant sites to the active zone in order to release neurotransmitter. This distant population of recycling vesicles is referred to as the reserve pool. 5. *Docking and Priming*. Proteins in the vesicular membrane must bind to specific partners in the plasma membrane, docking the vesicle to the active zone. Additional molecular events, collectively known as priming, must occur to render the vesicle competent for release. This population of docked and release competent recycling vesicles is known as the readily releasable pool.

1.4. VESICLE POOLS AND FM 1-43

There were few tools available to study vesicle recycling in live cells prior to the development of the fluorescent vesicle marker FM 1-43 by Betz and colleagues (Betz, Mao et al. 1992; Ryan 2001). This fluorescent molecule contains a long hydrophobic section with a positive charge at one end (Fig 3A). The hydrophobic region inserts into the outer leaflet of the cell membrane bilayer, while the positive charge prevents the molecule from crossing the membrane into the cell interior. During endocytosis this molecule becomes trapped inside newly formed vesicles, as the outer leaflet of the plasma membrane containing the dye becomes the inner leaflet of the vesicular membrane bilayer (Fig 3B). After endocytosis is complete, excess dye not incorporated into vesicles can be washed from the cell. The staining results in a punctate pattern (Fig 6 and Fig 16), where each spot corresponds to a synaptic bouton filled with many fluorescently labeled vesicles. Inducing exocytosis releases dye from the boutons and the fading of the fluorescent puncta (Fig 16). By imaging dye accumulation or depletion in the puncta under a variety of conditions, one can study various steps in the vesicle cycle. For example, experiments that measure the time for synapses to take up FM 1-43 dye during stimulation show that the typical time scale for endocytosis is ~40s (Ryan, Reuter et al. 1993). Once vesicles are loaded with dye, stimulating the synapse at 10 Hz, results in a decay in fluorescence with a typical time scale of ~20s (Ryan 1999; Fernandez-Alfonso and Ryan 2004). This represents the time needed to empty previously endocytosed vesicles from the bouton (steps 4 through 1 in Fig. 2). Also, Murthy and Stevens (1998) have demonstrated that the amount of dye taken up during endocytosis and released during exocytosis is quantized and equivalent, indicating that these vesicles do not fuse with intermediate structures such as endozomes (Murthy and Stevens 1998).

In addition to being a functional marker in live cells, this dye can be converted into an electron dense substance that can be visualized under electron microscopy, revealing the distribution of recycling vesicles (Fig 3C) (Harata, Pyle et al. 2001; Harata, Ryan et al. 2001; Schikorski and Stevens 2001). Together with earlier electrophysiological studies, these experiments demonstrate that vesicles in the bouton are divided into distinct functional pools. The first pool is called the readily releasable pool (RRP), which is available for exocytosis with little or no delay after the onset of electrical stimulation. These vesicles stain with FM 1-43 and are hypothesized to correspond to the 5 - 8 vesicles that are typically docked at the active zone. There exists a reserve pool (RP) that also labels with FM 1-43, but is at least twice as large as the RRP and is remote from the active zone. These RP vesicles are only available for exocytosis after some delay, which is on the order of several seconds or longer. Together the RRP and the RP form the recycling pool, which contains about 25-30 vesicles. Interestingly, the FM 1-43 studies reveal a large resting pool, containing about 170 vesicles, that does not label with dye even at saturating levels of fluorescent labeling. Therefore, the simplest explanation is that they do not participate in the vesicle cycle on the time scales accessible to these experiments. Why the synapse constructs a large population of resting vesicles is unclear. However, this notion that the synapse restricts the availability of vesicles for release is a reoccurring theme throughout the cycle, and our work shows that it holds for vesicle translocation as well where the majority of RP vesicles are bound and not available to join the RRP . This is particularly surprising since the demand for vesicles, imposed by the cell's electrical activity, often outstrips the supply of vesicles, which we discuss next.

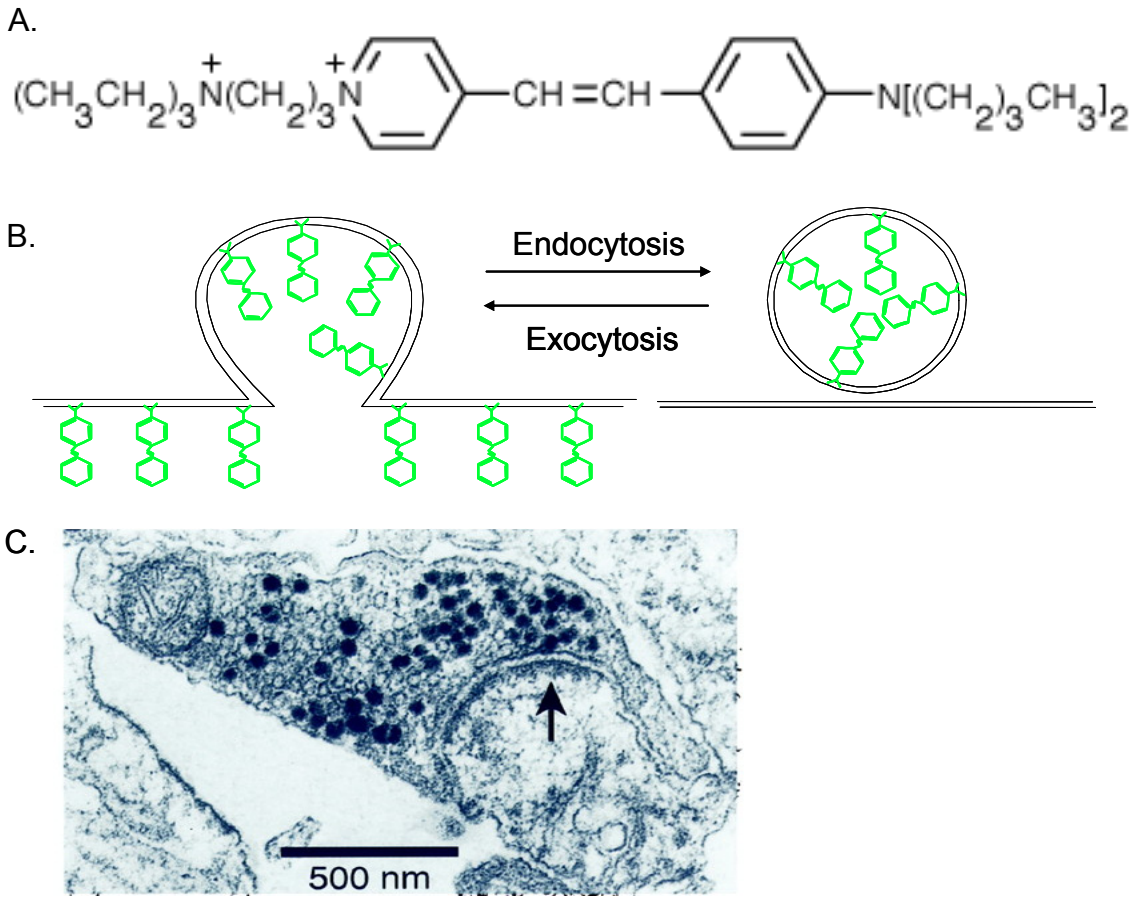

Figure 3 FM 1-43 is a marker for recycling vesicles. *A*. The structure of the fluorescent probe is ideal for labeling recycling vesicles. The right side of the molecule starting from the leftmost aromatic ring is hydrophobic and inserts into the plasma membrane. The two aromatic rings span a system of conjugated carbon double bonds, which can be lengthened to give the red shifted FM 4-64. The leftmost positive charge prevents the molecule from crossing the membrane and increases it solubility in water, allowing it to be delivered via the extracellular bath. *B*. Once in the bath, the dye binds the plasma membrane and is trapped in the vesicle during endocytosis. Afterwards, the excess dye can be washed away. During experiments that elicit exocytosis, the extracellular space is devoid of dye, which results in diffusion of dye away from the synapse. C, Electron micrograph adapted from Harata et. al. (2001) of a hippocampal synaptic bouton after it has been labeled at saturating levels with FM 1-43. The dye is trapped in recycling vesicles and becomes electron opaque after photo-conversion. Notice that many vesicles are clear and not labeled (resting pool) and the remaining labeled vesicles are either docked (RRP) or remote (RP) from the active zone (electron dense curved region of membrane above arrow).

1.5. VESICLE DEPLETION AND REFILLING

The mismatch between supply and demand of synaptic vesicles is thought to underlie a process called vesicle depletion. Perhaps the definitive study of this phenomenon was performed by Dobrunz and Stevens (1997). Using a well-known hippocampal brain slice preparation, they stimulated axons that are connected to a postsynaptic cell by a single synapse. Thus, in these experiments the electrical response recorded in the postsynaptic cell yields information about transmission at single synapses. The axon is stimulated with a series of action potentials at 10Hz and the excitatory post synaptic current (EPSC) is recorded for each stimulus. In between each round of action potentials the system is allowed to rest and resumes to its initial state. Figure 4A shows the probability of recording an EPSC in response to each stimulus in the train delivered to the presynaptic axon. First, notice that synaptic transmission is highly unreliable. The failure rate for even the first action potential in the train is typically over 50%. Synaptic boutons can also release neurotransmitter with low probability in the absence of stimulation, which is known as spontaneous release (Murthy and Stevens 1999). It is thought that this is due to the stochastic nature of vesicle fusion, where the probability of release is dependent on the internal Ca^{2+} concentration. This stochastic process makes synaptic transmission unreliable, and is thought to be the dominant source of noise in the brain (Allen and Stevens 1994; Stevens 1994; Rieke, Warland et al. 1998). Next, notice that the probability of release diminishes with each action potential in the train, reaching a steady state probability of about 5%. Upon cessation of the train of action potentials, the initial probability of release recovers in an exponential fashion with the average synapse recovering with a time scale of $\tau \approx 3$ sec. This process is referred to in the literature as refilling.

Much can be learned from this single experiment. First, Dobrunz and Stevens estimate the size of the RRP by counting the number of release events from t = 0 to the time where the probability drops to exp(-3) or ~5% of its original value. The calculation has two assumptions: 1) at most one vesicle is released per action potential and 2) minimal recovery occurs during the train of action potentials. The first assumption has experimental support (Stevens and Wang 1995; Hanse and Gustafsson 2001) and will be further justified below. The error in the second assumption will lead to an overestimation of the size of the RRP, which is small since the probability falls off fast compared to the recovery, with a decay time of ~0.5 s or about 6 times faster than the average refilling time of 3 s. The estimation of the size of the RRP was repeated for several synapses yielding an average maximum pools size of 8.8 ± 3.3 vesicles[1]. This agrees well with the average number of docked vesicles in this preparation, 10±5 measured via electron microscopy (Schikorski and Stevens 1997), confirming that the empirically defined RRP and the morphologically docked pool of vesicles are likely identical (Murthy and Stevens 1999). It should be noted that it is unclear whether vesicles that appear to be docked under electron microscopy actually sit at functional release sites or are able to undergo exocytosis. In fact, electron microscopy studies that label the entire recycling pool using FM 1-43 often contain several unlabeled vesicles that appear to be docked at the active zone. One possibility is that these vesicles undergo kiss-and-run and are unable to take up dye due the constriction of the hypothesized fusion pore. However, as we discuss in section 1.6, these must be rare events if they exist at all.

Dobrunz and Stevens also find that the initial release probability for the first action potential increases monotonically with the size of the RRP (Fig 4B), and can be modeled as a

[1] The size of the functional pool for a given synapse fluctuates from trial to trial. 8.8 represents the ensemble average of the maximum pool sizes measured for each synapse. The ensemble average of the typical pool sizes for each synapse is 5.5. It is this ensemble of typical pool sizes that is plotted in Fig.4B.

Poisson process where vesicles act independently in response to an action potential (Oertner, Sabatini et al. 2002). Thus, if there are ~10 docked vesicles on average and the probability of measuring a synaptic current does not exceed 50%, then the probability of a given vesicle releasing is less than 5% and that any two vesicles release in response to one action potential is well below 1%. Regardless of whether there exists a mechanism to block simultaneous release (Regehr and Stevens 2001) or if it is simply a rare event (Oertner, Sabatini et al. 2002), assumption (1) above is quite good.

What is the mechanism behind the phenomena above and what is its relationship to the vesicle cycle? It is hypothesized that as action potentials are delivered to the synapse, vesicles fuse with the plasma membrane decreasing the number of docked vesicles (RRP) and thus the probability of release. In addition, it is conjectured that refilling represents RP vesicles traveling to the active zone to join the RRP (Rosenmund and Stevens 1996). As a result, the release probability decreases rapidly when the RRP is depleted faster than the RP vesicles can refill it. This occurs even at the physiological stimulation frequencies used in these experiments. If this picture is accurate, then the movement of RP vesicles strongly influence the efficacy of synaptic transmission. However, as we discuss in section 1.7 this picture has yet to be confirmed.

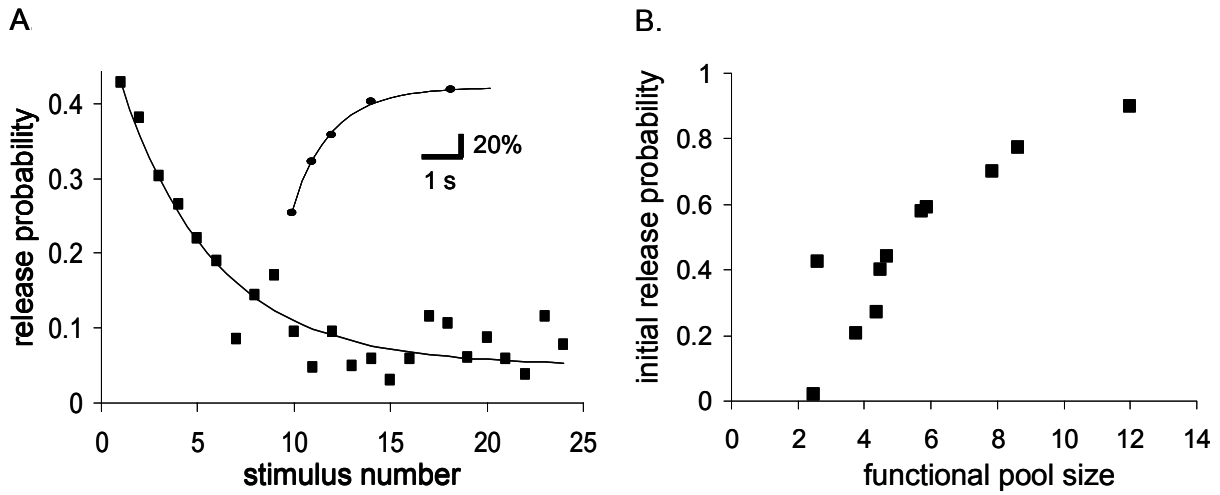

Figure 4 Vesicle Depletion adapted from Dobrunz and Stevens (1997). *A,* The probability of measuring neurotransmitter release decreases exponentially (τ = 4.9 stimuli) with each electrical stimulus given at 10Hz, reaching a steady state of about 5%. The 15th stimulus marks the time where the probability decays by 3 decay constants or exp(-3) of its original value. This empirically defines the point where one readily releasable pool worth of vesicles has been released. The inset shows the time course for a different synapse for the probability to recover to its original value after the stimulation has ceased. *B,* By integrating the probability from 0 to where it falls to exp(-3), one can measure the functional size of the readily releasable pool. Notice that the initial probability of releasing neurotransmitter increases with the size of the readily releasable pool, which is conjectured to correspond to the number of docked vesicles.

1.6. KISS-AND-RUN

In recent years, a growing body of evidence has been collected that suggests that there exists a shortcut for vesicle recycling, termed rapid endocytosis or "kiss-and-run" (Klingauf, Kavalali et al. 1998; Pyle, Kavalali et al. 2000; Stevens and Williams 2000; Aravanis, Pyle et al. 2003). In this process, vesicles release neurotransmitter without completely fusing with the plasma membrane. Some results indicate that during kiss-and-run, neurotransmitter release occurs through a protein channel called the fusion pore. This mechanism allows vesicles to remain intact and docked at the active zone, and to be rapidly refilled for the next action potential (Fig 2). This bypasses the slow endocytosis described in section 1.3 and the subsequent movement and docking to the active zone. This process is thought to alleviate the mismatch between the rate at which vesicles are depleted via exocytosis and the rate at which they are replenished via the RP, particularly at high stimulation frequencies (Pyle, Kavalali et al. 2000).

However, findings published by Fernandez-Alfonso and Ryan (2004) within the last year suggest that kiss-and-run has little impact on the supply of fusion competent vesicles at physiological stimulation frequencies. In fact, by revisiting the experiments described in the sections above we can see that this must be the case. First, recall that the number of docked vesicles is statistically indistinguishable from the functional size of the RRP. Each kiss-and-run event would increase the size of the empirically defined RRP by one, leaving the number of morphologically docked vesicles unchanged. Therefore, the difference between the two is an estimate of the number of kiss-and-run events that typically occur when the RRP is emptied. This difference is not significantly different from zero. Next, notice that the steady state probability of neurotransmitter release in Fig 4A is ~5%. Since the rate of stimulation is 10Hz, then the steady state rate of exocytosis is ~0.5 Hz. This agrees with the prediction of less than 1 Hz (section 1.3)

derived from the FM 1-43 studies described in section 1.4. If a significant number of vesicles could be rapidly recycled, it would increase the effective number of vesicles available for release beyond the 25-30 labeled vesicles observed under electron microscopy, and boost the steady state rate of exocytosis beyond 1 Hz. The lack of extra recycling capacity indicates that the kiss-and-run may be rare. Consistent with this, Stevens and Williams (2000) estimate that kiss-and-run makes up ~20 % of release events. Regardless of its frequency, the data suggests that kiss-and-run exocytosis has little effect on the supply of vesicles that are able to release neurotransmitter.

1.7. VESICLE MOTION

As we discussed in section 1.5, movement of RP vesicles to the active zone is hypothesized to have a large impact on synaptic transmission. However, little is known about the dynamics of these vesicles, particularly in the small synapses of the central nervous system where the number of recycling vesicles is highly restricted, and refilling of the small RRP is most critical.

Several studies hint that motor proteins may be involved in transporting vesicles to the active zone (Prekeris and Terrian 1997; Evans, Lee et al. 1998; Ryan 1999; Dresbach, Qualmann et al. 2001). The majority of these are biochemical studies showing that these proteins are bound to membranes of synaptic vesicles. There are few physiological studies that address the role of motor proteins in vesicle motion, and their results are not conclusive. For example, Ryan demonstrates that inhibiting a modulator of myosin, myosin light chain kinase, reduces the number of reserve vesicles available for exocytosis, but has no effect on kinetics (Ryan 1999). Prekeris and Terrian (1997) show that BDM, a pharmacological agent traditionally thought to specifically inhibit the myosin class of motors, severely inhibits synaptic transmission in

synaptosomes. This is a collection of cell fragments rich in intact synapses, and is not a live cell preparation. More importantly, BDM has recently been shown not to be specific for myosin proteins (Ostap 2002), and can depolymerize actin (Yarrow, Lechler et al. 2003), which is a structural protein polymer that has been implicated in vesicle motion. Hence, the role of motor proteins in vesicle transport in these synapses remains unclear.

Another important protein family implicated in vesicle transport is the Rab family of GTP-binding proteins. In particular, Rab3a-GTP and Rab3c-GTP bind synaptic vesicles at rest. Stimulation of vesicle exocytosis is associated with the release of Rab3a and Rab3c from vesicles and the hydrolysis of Rab3a-GTP to Rab3a-GDP. This binding is also modulated by Rab "effector" proteins such as GDI and rabphilin. Rab3a is also phosphorylated by multiple kinases, suggesting that its activity is phosphorylation dependent. Physiological experiments show that synapses of Rab3a knockout mice are able to release neurotransmitter upon stimulation, but show increased synaptic depression in response to sustained activity (Sudhof 1995). The detailed mechanism underlying this phenotype is unknown. However, it is hypothesized that the binding of Rab3 to actives zone proteins such as Munc18 is important for vesicle docking, which may be altered these mice. Regardless of the mechanism, the phenotype of Rab3 knockout mice suggests that these proteins regulate the availability of reserve pool vesicles.

There is also evidence that certain members of the Rab family interact with motor proteins. For example, Rab27a is responsible for the recruitment of myosinVa to melanosomes (Hume, Collinson et al. 2001), which are vesicular structures in the skin pigment producing cells called melanocytes. Rab6-GTP binds a kinesin type motor called Rabkinesin-6, which is important in the dynamics of the Golgi apparatus (Echard, Jollivet et al. 1998). Rab5 has been shown to promote association and transport of endosomes along microtubules (Nielsen, Severin

et al. 1999). Unfortunately, there is no evidence for the association of Rab proteins with motor proteins in synaptic vesicle transport.

The majority of work on vesicles dynamics has focused on the synapsin family of phosphoproteins (Sudhof 1995). Experiments performed in lamprey, squid, and *in vitro* show that these proteins tether a population of vesicles to actin filaments, one of the three components that make up the cytoskeleton (Benfenati, Valtorta et al. 1991; Greengard, Valtorta et al. 1993; Pieribone, Shupliakov et al. 1995). In response to Ca^{2+} entry into the synaptic bouton, these proteins become phosphorylated by a class of proteins called kinases (Chi, Greengard et al. 2001; Chi, Greengard et al. 2003). This releases vesicles from the cytoskeleton and is hypothesized to result in the movement of RP vesicles to the active zone to join the RRP. Supporting this idea, experiments that inject synapsin antibodies into lamprey reticulospinal axons, eliminate a population of vesicles remote from the active zone and inhibit exocytosis resulting from sustained stimulation (Pieribone, Shupliakov et al. 1995). During stimulation synapsin moves into the nearby axonal shaft, and returns to the bouton after the stimulation is halted (Chi, Greengard et al. 2001; Chi, Greengard et al. 2003). There also evidence that the Ca^{2+} entry and synapsin phosphorylation depolymerizes actin filaments, perhaps easing the subsequent movement of vesicles (Chieregatti, Ceccaldi et al. 1996).

Despite these observations, the role of synapsin and actin in the vesicle cycle is complex and controversial. A physical picture of how RP vesicles move to the active zone is still lacking, particularly in central synapses. First, studies on mice where the synapsin I and II genes have been removed, called “knock-out” mice show increased seizure propensity. However, synapses from these mice have normal synaptic structure and development. Although, repetitive stimulation of synapses lacking synapsin II show a form of decreased exocytosis, known as

"synaptic depression", these changes occur well before the docked pool is depleted (Sudhof 1995). This indicates that the role of synapsin may be to regulate exocytosis of already docked vesicles rather than the transport of reserve vesicles. Next, the role of actin in vesicle transport in hippocampal synapses has recently come into question. Sankaranarayanan et al. have shown that applying the drug latrunculin depolymerizes 98% of actin filaments in these synapses, but leaves the vesicle cluster intact and has little effect on the time needed to empty the recycling pool. (Sankaranarayanan, Atluri et al. 2003) The authors suggest that other structural proteins such as bassoon or piccolo may be involved in binding synaptic vesicles, rather than actin. However, whether these structural proteins interact with synapsin remains unclear.

The refilling of the RRP described in section 1.5, occurs in the absence of Ca^{2+} influx (Rosenmund and Stevens 1996), seemingly inconsistent with the synapsin model. In these refilling experiments, exocytosis is stimulated in a non-physiological manner by adding hypertonic sucrose solution to the bath (Stevens and Tsujimoto 1995; Dobrunz and Stevens 1997; Stevens and Sullivan 1998; Stevens and Wesseling 1998; Morales, Colicos et al. 2000; Pyle, Kavalali et al. 2000). The resulting change in extracellular osmolarity causes docked vesicles to fuse and release neurotransmitter through an unknown mechanism. Despite the lack of Ca^{2+} influx and subsequent phosphorylation of synapsin, the RRP still refills (presumably from the RP) with a similar exponential recovery to that observed in response to membrane depolarization, with relaxation times from 3-10s (Stevens and Tsujimoto 1995; Dobrunz and Stevens 1997). In addition, triggering action potentials and Ca^{2+} entry during the sucrose application results in only a moderate increase in the rate of refilling, with a decrease in τ, the typical refilling time, by a factor of 1.6 at 10Hz, and 1.8 at 50Hz (Stevens and Wesseling 1998). Other measurements by Wesseling and Lo (2002) also show that both electrical stimulation and

increasing calcium influx have little effect on the rate of refilling of the RRP. Surprisingly, applying a long train of action potentials prior to the application of sucrose, results in a double exponential time course for refilling, with the original 3-10s time scale intact and a new 60s time scale appearing (Liu and Tsien 1995; Stevens and Wesseling 1999). The source of this slow time scale is unknown, with one hypothesis being that docking sites become unavailable after sustained exocytosis (Stevens and Wesseling 1999).

Pyle et al. (2000) have conducted experiments which cast doubt on the current interpretation of refilling experiments. They provide evidence that the faster refilling process represents the exponential reloading of the RRP through kiss-and-run, and that the slow 60 s time scale actually represents the movement of RP vesicles to the active zone. They "avoid the ambiguous term 'refilling'" and conclude that their results "call for a revision of the prevailing conception of vesicle recycling." Evidence for this revision is growing with recent measurements demonstrating that synaptobrevin-2 is critical for rapid endocytosis, and refilling in synapses lacking this protein is three times slower than wild type synapses (Deak, Schoch et al. 2004). However, the majority of the experiments performed by Pyle et al (2000) were performed on synapses stimulated at 30 Hz, and more recent evidence shows that kiss-and-run has little or no contribution at frequencies closer to those observed *in vivo* (Fernandez-Alfonso and Ryan 2004).

Much of the controversy and ignorance that exists regarding the synaptic vesicle cycle stems from the fact that physiological studies on live synapses are only able to measure exocytosis. Typically, one can only infer information about the vesicle cycle by observing its final output, without being able to probe the individual steps and mechanisms of the pathways that lie within the bouton. In this thesis we utilize a variety of optical techniques to study vesicle motion, a crucial process within the vesicle cycle, inside individual living synapses.

These studies show that when the cell is electrically at rest, only a small population of reserve pool vesicles is mobile, taking seconds to traverse the synapse. This sluggish motion is due to phosphorylation dependent binding of vesicles to structural proteins within the synapse. We also find that a simple stick-and-diffuse model (Fig 16) can account for our experimental results, and also predicts the well-known exponential refilling of the readily releasable pool. This suggests that the movement of vesicles to the active zone is the rate limiting step in this process.

2. EXPERIMENTAL TECNIQUES

Many of the ideas about vesicle movement are built from the empirical observations of vesicle refilling experiments (section 1.5). The time scale for recovery in these experiments encompass several processes within the vesicle cycle including movement, docking, priming and release of vesicles (Sudhof 1995). Using conventional approaches, the dynamics and regulation of these processes cannot be separated. Hence, the study of vesicle movement requires more direct measurements of synaptic vesicle motion. However, studying vesicle dynamics in most central nervous system synapses is challenging primarily due to the bouton's size. These small (~0.1μm^3) boutons are packed with hundreds of synaptic vesicles that are approximately 40 nm in diameter, which is well below the diffraction limit of visible light. Therefore, imaging synaptic vesicles directly using light microscopy is problematic (Aravanis, Pyle et al. 2003). Instead, we use fluorescence correlation spectroscopy (FCS) and fluorescence recovery after photobleaching (FRAP) to study vesicle dynamics in small central synapses for the first time. The technical details of these two techniques are the focus of this chapter. Several less complicated experimental procedures utilized in this work are included at the end if this chapter in less detail.

2.1. FLUORESCENCE CORRELATION SPECTROSCOPY

Fluorescence correlation spectroscopy (FCS) was developed in Watt Webb's lab in the early 1970's (Magde, Elson et al. 1972) originally to probe the dynamics of chemical reactions. Today, this technique utilizes fluctuations primarily to study the motion of particles (Kricevsky and Bonnet 2002), similar to its predecessor, quasi-elastic light scattering. In FCS, a laser beam is focused by converging optics to a diffraction limited spot within the sample. The sample contains objects tagged with fluorescent molecules, whose emission is excited by the laser beam. The image of the resulting fluorescent spot is projected onto a pinhole, which rejects out of focus light and reduces the volume of fluorescent objects from which the detector collects photons. Together the laser, the collection optics, and the pinhole determine the size of the detection volume or "light-box". This configuration is known as a confocal geometry and is utilized in a variety of commercially available microscopes. However, unlike typical confocal microscopy, FCS does not image the sample and thus does not require spatial scanning. Instead, FCS records the fluorescence intensity of the sample as a function of time. The fluorescence intensity I(t) is proportional to the number of fluorescent objects in the detection volume N(t). As fluorescent objects move about the sample, the number of objects in the light-box and the measured fluorescence intensity will fluctuate with time. Different types of motion will yield different statistics for these fluctuations. The job of the investigator is to infer the dynamics of the particles from these statistics. This analysis most commonly involves calculating the intensity-intensity autocorrelation function $G(\tau) = \langle \delta I(t) \delta I(t+\tau) \rangle / \langle I(t) \rangle^2$, where $\delta I(t) = I(t) - \langle I(t) \rangle$ and $\langle \ldots \rangle$ represents a time average. Here, $G(\tau)$ quantifies the correlation between pairs of fluorescence intensity fluctuations observed τ seconds apart. As vesicles redistribute, these correlations decay and provide information about the underlying dynamics. Note for $\tau = 0$, the

amplitude of the autocorrelation function $G(0) = \langle \delta I(t)^2 \rangle / \langle I(t) \rangle^2 = \langle \delta N(t)^2 \rangle / \langle N(t) \rangle^2$, which is simply the variance of the number of fluorescent particles in the light-box.

Diffusion is a common form of dynamics observed throughout nature, and serves as a simple model to discuss and gain intuition about FCS. Consider a freely diffusing fluorescent species whose local concentration fluctuates $\delta c(\vec{r},t) = c(\vec{r},t) - \langle c(\vec{r},t) \rangle$. Here $\langle c(\vec{r},t) \rangle$ is an ensemble average concentration. These concentration fluctuations obey the diffusion equation:

$$\frac{\partial \delta c(\vec{r},t)}{\partial t} = D\nabla^2 \delta c(\vec{r},t) \qquad (1)$$

The fluorescence intensity I_f reaching the detector is:

$$I_f(t) = Q\varepsilon \int I_e(\vec{r}) c(\vec{r},t) d^3 r \qquad (2),$$

where ε and Q are, respectively, the extinction coefficient (probability of photon being absorbed) and the quantum yield (probability of relaxing to ground state via photon emission given an excitation). I_e describes the size of the detection volume, and is often referred to as the excitation intensity profile. The deviation of the fluorescence intensity from the mean is:

$$\delta I_f(t) = Q\varepsilon \int I_e(\vec{r}) \delta c(\vec{r},t) d^3 r \qquad (3)$$

As mentioned above FCS experiments typically measure the intensity-intensity autocorrelation function, normalized by the mean intensity squared:

$$G(\tau) = \frac{\langle \delta I_f(t) \delta I_f(t+\tau) \rangle}{\langle I_f(t) \rangle^2} \qquad (4),$$

where <…> represents a time average. To continue further we must assume ergodicity, where the time average can be replaced by an ensemble average. In addition if the system is stationary, then the correlation function only depends on the relative time difference τ and not the absolute time, t. Now we can substitute equations (2) and (3) into equation (4) giving:

$$G(\tau) = \frac{(Q\varepsilon)^2}{\langle I_f(t)\rangle^2} \int\int I_e(\vec{r}) I_e(\vec{r}') \langle \delta c(\vec{r},0)\delta c(\vec{r}',\tau)\rangle d^3 r d^3 r' \qquad (5)$$

By utilizing the Fourier transform $\delta c(\vec{r},t) = 1/(2\pi)^3 \int \delta c(\vec{q},t) e^{i\vec{q}\bullet\vec{r}} d^3 q$ we can rewrite equation (5) to read:

$$G(\tau) = \frac{(Q\varepsilon)^2}{\langle I_f(t)\rangle^2 (2\pi)^3} \int\int I_e(\vec{q}) I_e(\vec{q}') \langle \delta c(\vec{q},0)\delta c(\vec{q}',\tau)\rangle d^3 q d^3 q' \qquad (6),$$

where $I_e(\vec{q}) = \int I_e(\vec{r}) e^{-i\vec{q}\bullet\vec{r}} d^3 q$.

Using the inverse Fourier transform $\delta c(\vec{q},t) = \int \delta c(\vec{r},t) e^{-i\vec{q}\bullet\vec{r}} d^3 r$, one can rewrite the correlation function inside the integral to:

$$\langle \delta c(\vec{q},0)\delta c(\vec{q}',\tau)\rangle = \int d^3 r \int d^3 r' \langle \delta c(\vec{r},0)\delta c(\vec{r}',\tau)\rangle e^{-i(\vec{q}\bullet\vec{r}+\vec{q}'\bullet\vec{r}')} \qquad (7).$$

If one assumes the systems is homogeneous and isotropic then equation (7) only depends on the separation $\vec{R} = \vec{r} - \vec{r}'$ and one can transform the variables from $\vec{r},\vec{r}'$ to $\vec{r},\vec{R}$. One can then rearrange terms to yield a product of two independent integrals, one that contains only $\vec{r}$ and is the Dirac delta function and the other contains only $\vec{R}$. They simplify to:

$$\langle \delta c(\vec{q},0)\delta c(\vec{q}',\tau)\rangle = \delta(\vec{q} - \vec{q}') \langle \delta c^*(\vec{q},0)\delta c(\vec{q},\tau)\rangle \qquad (8)$$

Substituting equation (8) into equation (6) gives:

$$G(\tau) = \frac{(Q\varepsilon)^2}{\langle I_f(t)\rangle^2 (2\pi)^3} \int |I_e(\vec{q})|^2 \langle \delta c^*(\vec{q},0)\delta c(\vec{q},\tau)\rangle d^3 q \qquad (9)$$

Next we solve the diffusion equation via the Fourier method by substituting $\delta c(\vec{r},t) = 1/(2\pi)^3 \int \delta c(\vec{q},t) e^{i\vec{q}\bullet\vec{r}} d^3 q$ into both sides of equation (1) and utilizing orthogonality to give:

$$\frac{\partial \delta c(\vec{q},t)}{\partial t} = \left(i|\vec{q}|\right)^2 D\delta c(\vec{q},t) = -|\vec{q}|^2 D\delta c(\vec{q},t) \qquad (10)$$

It can easily be verified that the solution to equation (10) is $\delta c(\vec{q},t) = \delta c(\vec{q},0)e^{-D|\vec{q}|^2 t}$. Therefore

$$\left\langle \delta c^*(\vec{q},0)\delta c(\vec{q},\tau)\right\rangle = \left\langle |\delta c(\vec{q})|^2 \right\rangle e^{-D|\vec{q}|^2 t} \qquad (11)$$

Before substituting this into equation (9), we will consider the excitation intensity profile. Typically it has a Gaussian profile with the following form:

$I_e(\vec{r}) = I_0 \exp\left[-\frac{\left(x^2+y^2\right)}{2w_{xy}^2}\right]\exp\left[-\frac{z^2}{2w_z^2}\right]$ with its Fourier transform equal to

$$I_e(\vec{q}) = \left(2\pi\right)^{3/2}\sigma_{xy}^2\sigma_z I_0 \exp\left[-\frac{1}{2}\left(q_x{}^2 + q_y{}^2\right)w_{xy}^2\right]\exp\left[-\frac{1}{2}q_z{}^2 w_z^2\right]$$

$$= I_e(\vec{q}=0)\exp\left[-\frac{1}{2}\left(q_x{}^2 + q_y{}^2\right)w_{xy}^2\right]\exp\left[-\frac{1}{2}q_z{}^2 w_z^2\right] \qquad (12)$$

Here the w_i is the Gaussian radius of the excitation intensity profile along dimension *i*. Typically, $w_z > w_x = w_y \equiv w_{xy}$. Also, taking the average of both sides of equation (2) yields:

$$\left\langle I_f(t)\right\rangle = Q\varepsilon\int I_e(\vec{r})\left\langle c(\vec{r},t)\right\rangle d^3r = Q\varepsilon\left\langle c(\vec{r},t)\right\rangle\int I_e(\vec{r})d^3r = Q\varepsilon\left\langle c(\vec{r},t)\right\rangle I_e(\vec{q}=0) \qquad (13)$$

Now we can substitute equations (11), (12), and (13) into equation (9):

$$G(\tau) = \frac{\left\langle |\delta c|^2\right\rangle}{\left(2\pi\right)^3\left\langle c(\vec{r},t)\right\rangle^2}\int \exp\left[-\left(q_x{}^2 + q_y{}^2\right)w_{xy}^2\right]\exp\left[-q_z{}^2 w_z^2\right]\exp\left[-D\left(q_x{}^2 + q_y{}^2 + q_z{}^2\right)t\right]d^3q$$

$$= \frac{\left\langle |\delta c|^2\right\rangle}{\left\langle c(\vec{r},t)\right\rangle^2}\left[1+\frac{\tau}{\tau_{xy}}\right]^{-1}\left[1+\frac{\tau}{\tau_z}\right]^{-1/2} = \frac{\left\langle |\delta N|^2\right\rangle}{\left\langle N\right\rangle^2}\left[1+\frac{\tau}{\tau_{xy}}\right]^{-1}\left[1+\frac{\tau}{\tau_z}\right]^{-1/2}$$
$$= \frac{1}{\left\langle N\right\rangle}\left[1+\frac{\tau}{\tau_{xy}}\right]^{-1}\left[1+\frac{\tau}{\tau_z}\right]^{-1/2} \qquad (14),$$

where $\tau_i = \frac{w_i^2}{D}$ is the correlation time. Here we have used the fact that $\left|\delta c(\vec{q})\right|^2$ is independent of $\vec{q}$ for $\left|\vec{q}\right|^{-1}$ greater than the mean free path of the fluorescent object, which is typically of order 1 nm. Also, the particle number fluctuations obey statistics of the grand canonical ensemble and are Poissonian, where $\left\langle \left|\delta N\right|^2 \right\rangle = \left\langle N \right\rangle$.

Next we describe the implementation of, and the technical challenges involved in using FCS to investigate the dynamics of FM 1-43 labeled vesicles in the hippocampal neuronal culture. The experiments were performed on an inverted epifluorescence microscope, using a 100x 1.3 N.A. oil immersion lens (item 14 in Fig 5). The fluorescent attachment and Xenon arc lamp (7) were removed, exposing the back port of the microscope, and allowing both the Argon laser (1) beam (λ = 488 nm, ~0.5 μW) and the light from the arc lamp to be launched into the microscope through a 50/50 beam splitter (11). The light emerging from the fluorescent attachment is divergent, and the optical path length from the attachment to the back port must be maintained to achieve high quality illumination. This is accomplished by projecting the image of the fluorescent attachment to its normal position behind the microscope using a converging lens (10). Individual labeled synapses were visualized and selected under wide field illumination and then positioned onto the argon laser spot by moving a manual or a motorized microscope stage. However, the laser spot cannot pass the emission filter (15) mounted in the filter cube and is not visible to the experimenter, making the positioning of the fluorescent synapse nearly impossible. To solve this problem, we introduced a red HeNe (λ = 632 nm) laser (2) beam to mark the position of the excitation spot. Both laser beams were combined using a dichroic mirror (5) and launched into a single mode (488nm) optical fiber (6) with collimating optics. Single mode fibers can propagate beams with wavelengths longer than the optimal wavelength with some distortion

and attenuation. This is acceptable for the HeNe beam, which was utilized only as a marker for the Argon beam. However, to launch the HeNe laser into the microscope, the excitation filter (8) must be removed from the filter cube and mounted separately in front of the fluorescent attachment. This allows both laser beams and the light from the arc lamp to reach the sample. Although, the dichroic mirror (13) (497LP) mounted in the filter cube attenuates >90% of the HeNe laser intensity, the beam is still visible. It is important to note that this configuration must be modified when performing experiments utilizing two or more dyes with non-overlapping excitation spectrums. The fluorescence is collected using the same infinity corrected objective (14) that focuses the excitation light, and is then focused by a converging lens (16) onto a 50 μm pinhole (18) placed in the side port. The fluorescence intensity is measured using an avalanche photodiode (APD) (19) and the photon counts are recorded using an autocorrelator.

2.2. FLUORESCENCE RECOVERY AFTER PHOTOBLEACHING

Fluorescence recovery after photobleaching (FRAP) was also developed in the Webb lab shortly after the development of FCS (Schlessinger, Koppel et al. 1976). Again using a confocal geometry, an intense laser beam is used to destroy or "photobleach" a high percentage of the fluorescent molecules within the light-box, creating a void of fluorescent objects. As the remaining fluorescent objects redistribute, the average movement occurs down the concentration gradient, and the fluorescence intensity recovers. Compared to FCS, it is more suited for measuring slow dynamics. To see this, consider a system of diffusing particles with diffusion constant D. Recall, that the correlation time for the system is $\tau = w_{xy}^2/D$. In practice, FCS requires that the total measurement time T to be orders of magnitude longer than the correlation

time, where the signal to noise ratio[2] increases as $T^{1/2}$. In contrast, depending on the bleaching intensity and profile of the laser beam, the FRAP experiment on the same particles yields a fluorescence recovery resembling an exponential $[1 - \exp(-t/\tau)]$. To characterize the recovery curve, the measurement time need only be a few τ. For example, consider a system with a correlation time of 10 s, which is not unusual in biological systems. The FCS experiment requires about 15 minutes, where as a FRAP experiment on the same system can be completed in less than a minute. This difference can be critical in biological systems because living samples often deteriorate. In addition, biological systems are often heterogeneous and lack ergodicity, requiring one to gather statistics on an ensemble of samples. FCS studies in biological systems become impractical, if not impossible, as correlation times approach and exceed 10s.

The experimental setup for FRAP is identical to the one used for FCS, with some added components (Fig 5). First, the intensity of the excitation beam was increased to ~100 μW for ~0.5 s to bleach the synapse by moving a neutral density filter (3) out of the light path using a solenoid actuator. This combination of exposure time and excitation intensity decreased the intensity measured by the APD in the light box by 64.60±0.05 %, while the total intensity of the FM 1-43 labeled synapse (measured by the camera) decreased by only 13±2 %. Also, during the time that the excitation intensity was transiently increased, the APD was blocked by a shutter (17) to avoid saturation that can not only damage the detector, but also yield transients that can be mistaken for a FRAP signal. The fluorescence intensity recorded by the autocorrelator prior to bleaching I_{pre} was averaged for 5 s. In these experiments, t = 0 marks the time that the bleaching was completed. Approximately 100 ms later, the APD was unblocked and the fluorescence

[2] While shot noise does not contribute to $G(\tau)$, it does contribute to the noise in $G(\tau)$. For FCS, the signal to noise ratio $S/N = G(\tau)/(\Delta G(\tau)^2)^{1/2} = G(\tau)\langle N\rangle\nu T^{1/2}$, where ν is the number of fluorescent photons collected per particle per sampling time. Note that $G(\tau)$ is proportional to $1/\langle N\rangle$, and the S/N is independent of the concentration.

intensity I(t) was recorded. The fraction recovery was calculated as $R(t) = [I(t) - I(0)]/[I_{pre} - I(0)]$.

2.3. REMAINING EXPERIMENTAL TECHNIQUES AND PROTOCOLS

Primary cell culture. Cultures of dissociated embryonic rat hippocampal neurons were prepared as described previously (Bi and Poo 1998). Cells were used for experiments after 12-18 days in culture.

Fluorescence Labeling. The culture was constantly perfused at room temperature with a HEPES-buffered saline (HBS) solution containing the following (in mM): NaCl 150, KCl 3, $CaCl_2$ 3, $MgCl_2$ 2, HEPES 10, glucose 5, and pH 7.3, for all experiments unless stated otherwise. Synapses were loaded with dye by perfusing cells with HBS containing 10-15μM FM 1-43 (Synaptogreen, Biotium, Hayward, CA) and 50-90 mM KCl for 60 s, followed by perfusion with HBS containing only dye for 30 s. This was followed by a fast perfusion of dye-free (typically Ca^{++}-free) HBS for 10 min at a rate greater than 2 ml/min. In some experiments, 300 μM ADVASEP-7 (Biotium) was added for one minute to the dye-free HBS, beginning one minute after the initiation of the fast perfusion (Kay, Alfonso et al. 1999). The majority of images of FM 1-43 puncta were taken with a Hamamatsu C9100-12 CCD camera, using the same microscope and fluorescent filters as described for FCS below.

Fixation. Synapses used in experiments with fixed cells were loaded with the fixable version of FM 1-43, AM 1-43 (Biotium) using a similar protocol to the one described above. Cells were then placed in 4 percent paraformaldehyde for 30 minutes, followed by rinsing several times in phosphate buffered saline (PBS). Cells were stored in PBS up to the time of the experiment.

Additional FCS Details. The Gaussian detection volume or the "light-box" ($e^{-r^2/2w^2}$) with a radius w = 0.11 μm, was calibrated by performing FCS on dyes with a known diffusion coefficient. This radius is consistent with the size of the confocal detection volume measured by scanning subresolution (40 nm) fluorescent beads (Fig. 6C). This radius represents the distance that a freely diffusing object must traverse for the correlation function to decrease by 50% (Berne and Pecora 2000). The raw fluorescence intensity I(t) was typically binned to >10 ms and then fit to an exponential curve $I_B=I_0\exp(-t/t_B)$, which accounts for the photobleaching (typically t_B > 200s). The fluorescence intensity-intensity autocorrelation function $G(\tau) = \langle\delta I(t)\delta I(t+\tau)\rangle/\langle I(t)\rangle^2$ was calculated, where $\delta I=I(t)-I_B$ and <…> represents a time average.

Okadaic Acid. 2 μM Okadaic acid (OA) (LC Laboratories, Woburn, MA), diluted from frozen stock solutions aliquoted in DMSO, was added after dye loading such that the final concentration of DMSO did not exceed 0.1% to avoid DMSO toxicity. For experiments using OA, regions of interest (ROI) were drawn around synapses that appear as fluorescent puncta, as well as neuronal processes labeled nonspecifically. Normally, nonspecific labeling is estimated by measuring the fluorescence remaining in puncta after exhaustive exocytosis (Appendix). Since vesicle exocytosis may be altered by OA, background regions were averaged and compared to puncta to estimate the non-vesicular contribution to the synapses' fluorescence for both control and OA exposed synapses. A decrease in background fluorescence was observed upon addition of OA. This secondary effect cannot be attributed to photobleaching. The fading in puncta greatly exceeded this change in background. The difference between fading in the synapses and fading in the background was attributed to loss of vesicles.

Synapse size. We measured synapse size by scanning individual puncta via scanning stage confocal microscopy as shown in Fig. 6C. However, this process is rather slow. To gather

sufficient statistics, synapse area was measured by plotting the intensity along the long and short axes of camera images of fluorescent puncta. The baseline intensity was subtracted from each intensity profile and the full width half maximum (FWHM) was calculated. The intensity profile was approximated as a Gaussian function, allowing the FWHM to be converted to a Gaussian radius w_I. Due to diffraction, the image is not an exact representation of the synapse in the object plane. Mathematically, the image intensity profile represents the actual synapse shape profile convolved by the point spread function (PSF) of the microscope (Fig 18B). If all three profiles are assumed to be Gaussian, than the radius w_s along a given axis s of the synapse can be estimated as $w_s^2 = w_I^2 - w_{PSF}^2$, where w_{PSF} is the Gaussian radius of the PSF. The synapse and light-box area were calculated by approximating the synapse as an ellipse of area $A = \pi w_{short} w_{long}$ and the light-box as a circle of area $A = \pi w^2$.

Synaptic Motion. Synaptic boutons are dynamic structures, whose shape and size evolve with time (Colicos, Collins et al. 2001). Such synaptic motion could contribute to the measurement of fluorescence intensity fluctuations and fluorescence recovery, as the fluorescent synapse moves relative to the fixed laser beam. To determine the contribution of this motion, we used video fluorescence microscopy to record the center of mass position of individual synapses labeled with FM 1-43. The video rate was 3 frames per second. This measurement was compared to the intrinsic drift of the experimental setup by recording the position as a function of time of 0.42 μm diameter FITC labeled beads adsorbed onto a glass cover-slip. Puncta and beads were identified by hand and the center of mass position $\vec{r}_{cm} = \sum_i I_i \vec{r}_i \Big/ \sum_i I_i$ for each 1x1μm^2 ROI containing a punctum was calculated for each frame, where I_i and $\vec{r}_i$ are the fluorescence intensity and position respectively of the ith pixel in the ROI. The average $<\Delta r^2(t)>$ was

calculated for 30 synapses and is plotted versus t in Fig. 10B. The slope of this line is equal to $4D_{CM}$, where the effective diffusion coefficient of the center of mass $D_{CM} = 5.4 \times 10^{-15}$ cm^2/s. As will be shown below this diffusion coefficient is about three orders of magnitude smaller than the vesicle dynamics measured by FCS or FRAP.

Mechanical Perturbations. Synapses were labeled with FM 1-43 positioned onto the laser spot as described above. A glass micropipette filled with extracellular fluid and with a ~2 μm opening was positioned 1-2 μm from a labeled bouton. A 4 ms (Δ) and 4-6 PSI puff was applied with a picospritzer (Parker Instrumentation) every 1.5 seconds, and the fluorescence intensity was recorded by the APD and autocorrelator. TTL pulses marking the position of the puffs were simultaneously recorded by the autocorrelator in the second channel. The forcing time trace F(t) with an amplitude $F_0 = 1$ was crosscorrelated with the change in fluorescence intensity δI(t) to give the crosscorrelation function $G_{cross}(\tau) = \langle \delta F(t) \delta I(t+\tau) \rangle / (\langle F(t) \rangle \langle I(t) \rangle)$, where again <…> represents a time average. Since the pulses are spaced far apart, this is simply a pulse triggered average of δI(t).

The crosscorrelation functions from individual synapses were averaged and the average crosscorrelation function was fit to a phenomenological model of the dynamics constructed using a one dimensional forced simple harmonic oscillator (Marion and Thorton 1995), with the following equation of motion:

$$\ddot{x} + 2\beta\dot{x} + \omega_0^2 x = A(t), \text{ where } \beta = b/2m \quad \omega_0 = \sqrt{k/m} \quad A(t) = F(t)/m$$

Here, b is the viscosity, m is the mass, and k is the spring constant. $F(t)$ is an impulse function delivered at time $t = t' = 0$ of width Δ, with the amplitude F_0. The solution is found by solving for the Green's Function:

$$G(t,t') = \frac{e^{-\beta(t-t')}}{\omega'}\sin(\omega'(t-t'))$$

and solving for $x(t) = \int_{-\infty}^{\infty} F(t')G(t,t')dt'$. Here $\omega = i\beta' = i\sqrt{\beta^2 - \omega_0^2}$. In the over-damped case:

$$x_j(t) = \frac{F}{2m\omega_0^2\beta'}\left\{\left(\beta+\beta'\right)e^{-(\beta-\beta')t}\left(1+e^{(2\beta-\beta')\Delta}\right)-\left(\beta-\beta'\right)e^{-(\beta+\beta')t}\left(1+e^{(2\beta+\beta')\Delta}\right)\right\}$$

This function has two relaxation times, one fast $\tau_{fast} = \left(\beta+\beta'\right)^{-1}$ and one slow $\tau_{slow} = \left(\beta-\beta'\right)^{-1}$.

All errors and error bars represent the standard error of the mean (SEM), unless stated otherwise.

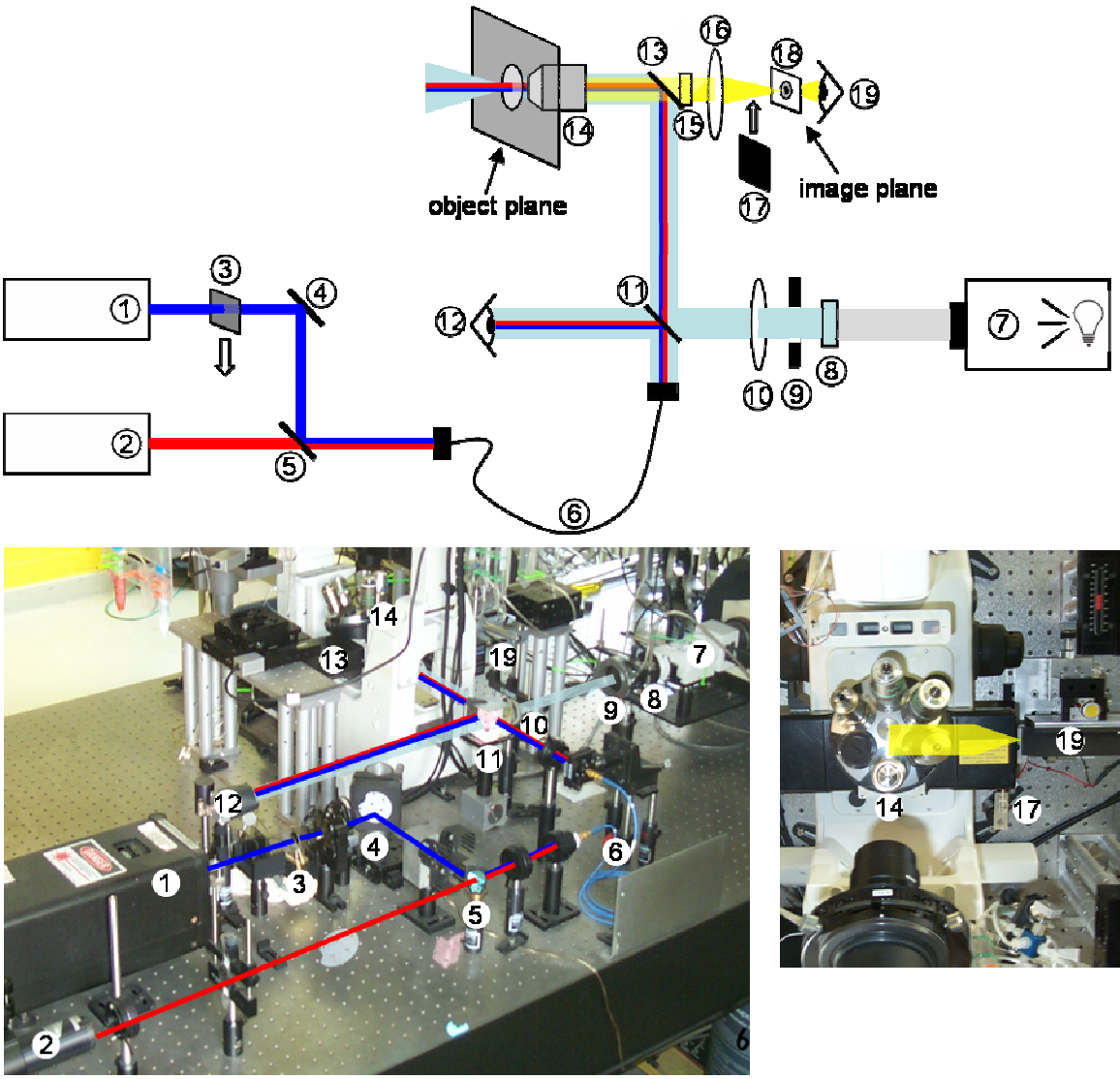

Figure 5 FCS and FRAP Experimental Setup

1. Argon laser (488 nm)
2. HeNe laser (632 nm) with kinematic mount
3. neutral density filter with actuator
4. mirror with kinematic mount
5. dichroic beam splitter (580DCXR)
6. single mode (488 nm) optical fiber
7. arc lamp & fluorescence attachment (Nikon TE-FM)
8. excitation filter (D470/40)
9. mechanical shutter
10. converging lens (f = 30cm)
11. 50/50 beam splitter
12. photodiode
13. dichroic beam splitter (Q497LP)
14. 100x 1.3 NA objective
15. emission filter (HQ510LP)
16. side port converging lens
17. shutter with actuator
18. 50 µm pinhole
19. avalanche photodiode

3. EXPERIMENTAL RESULTS I: NATIVE VESICLE DYNAMICS

3.1. ESTABLISHING THE FCS TECHNIQUE IN SINGLE SYNAPSES

A typical synaptic vesicle FCS measurement is depicted in Fig. 6. Here the neuronal culture is stimulated with a high K^+ solution while FM 1-43 is added to the bath. The excess dye is subsequently washed away and the resulting fluorescence appears as a punctuate pattern along neuronal processes (Fig 6A). Each fluorescent spot or punctum represents a synaptic bouton filled with many fluorescent vesicles. Figure 6B depicts the laser spot and detection volume (light-box) positioned onto one of the typical large synaptic boutons. It is important that vesicles can leave the light-box for fluorescence intensity fluctuations to be observed. The synapse thickness is significantly smaller than the height of the light-box, and the motion perpendicular to the coverslip is not detected. The lateral dimensions of the synaptic bouton in Fig 6B are measured by scanning the detection volume across the synapse, which are displayed in Fig. 6C. The narrowest dimension of the bouton is less than twice the size of the light-box. This natural confinement can be taken into account, and the vesicles appear as if they are moving in a constrained two dimensional system (Gennerich and Schild 2000). Measuring the area of synaptic boutons in this manner is cumbersome, making it difficult to gather sufficient statistics. Therefore, the area of an ensemble of labeled synapses was measured from camera images corrected for convolution effects, resulting in an average area of $0.34\pm0.02\ \mu m^2$ (n = 33). This area is 9±2 times larger than the area of the light-box ($0.038\pm0.009\ \mu m^2$), and is consistent with

the average cross sectional area of approximately 0.3 μm^2 measured from electron micrographs of cultured hippocampal synaptic boutons (Schikorski and Stevens 2001). This ratio of synapse to light-box size is also consistent with photometric calibrations that show that the total amount of fluorescence emanating from these synapses is an order of magnitude larger than the fluorescence measured in a typical FCS measurement (Appendix). In the FCS and FRAP measurements, we also took advantage of the great heterogeneity in bouton sizes (Schikorski and Stevens 1997) by selecting the largest and brightest puncta. Hence, the light-box is small enough that vesicles can exit this volume, which is required for observing fluorescence fluctuations.

There exists the possibility that the largest and brightest puncta in the field of view may not be functional synapses. For example, the soma of certain cells, beading or varicosities in non-healthy neuronal processes, and vesicular structures within healthy glial cells also take up FM 1-43 under certain conditions (Fig 7). Although these can easily be identified and avoided by an experienced experimenter, other sources of nonsynaptic labeling may be more subtle. To address this issue, we examined if there is a correlation between the fluorescence intensity of a punctum and the amount of fluorescence it looses upon subsequent stimulation (unloading). Functional synapses are filled with release competent vesicles, which exocytose and loose dye upon stimulation. In contrast, nonsynaptic puncta and nonviable synapses are not functional and should have no change upon stimulation. Figure 8 shows that the fraction of fluorescence remaining after a second round of stimulation decreases as a function of the starting intensity. Thus, the brightest puncta unload the highest percentage of dye and are indeed functional synapses.

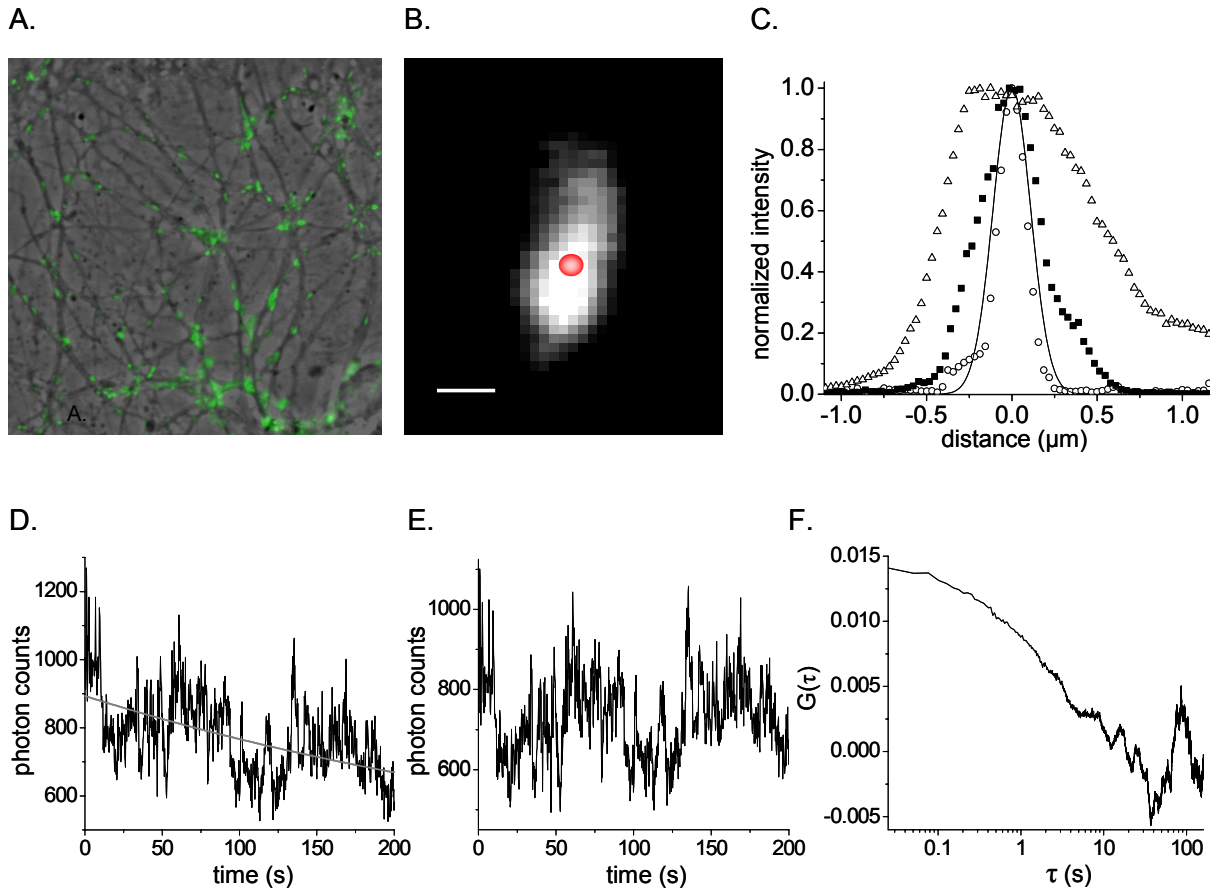

Figure 6 FCS measures vesicle dynamics in single synapses. *A*, The fluorescence intensity of FM 1-43 labeled synaptic boutons lie along neuronal processes in the phase contrast image. *B*, A schematic of the FCS detection volume (light-box) is shown overlying a typical large synapse labeled with the FM 1-43 (scale bar 0.5 μm). *C*, A plot of the normalized intensity measured by scanning the detection volume along the long (open triangles) and the short (closed squares) axes of this synapse as well as a 40 nm fluorescent bead (open circles). A plot of the Gaussian light-box $I=I_0\exp(-r^2/2w^2)$ (solid line), where w = 0.11 μm, is also shown. *D*, The intensity trace measured from a single synapse is fit to an exponential function (gray line). *E*, This trace is corrected for photobleaching and is used to calculate the autocorrelation function G(τ) shown in *F*.

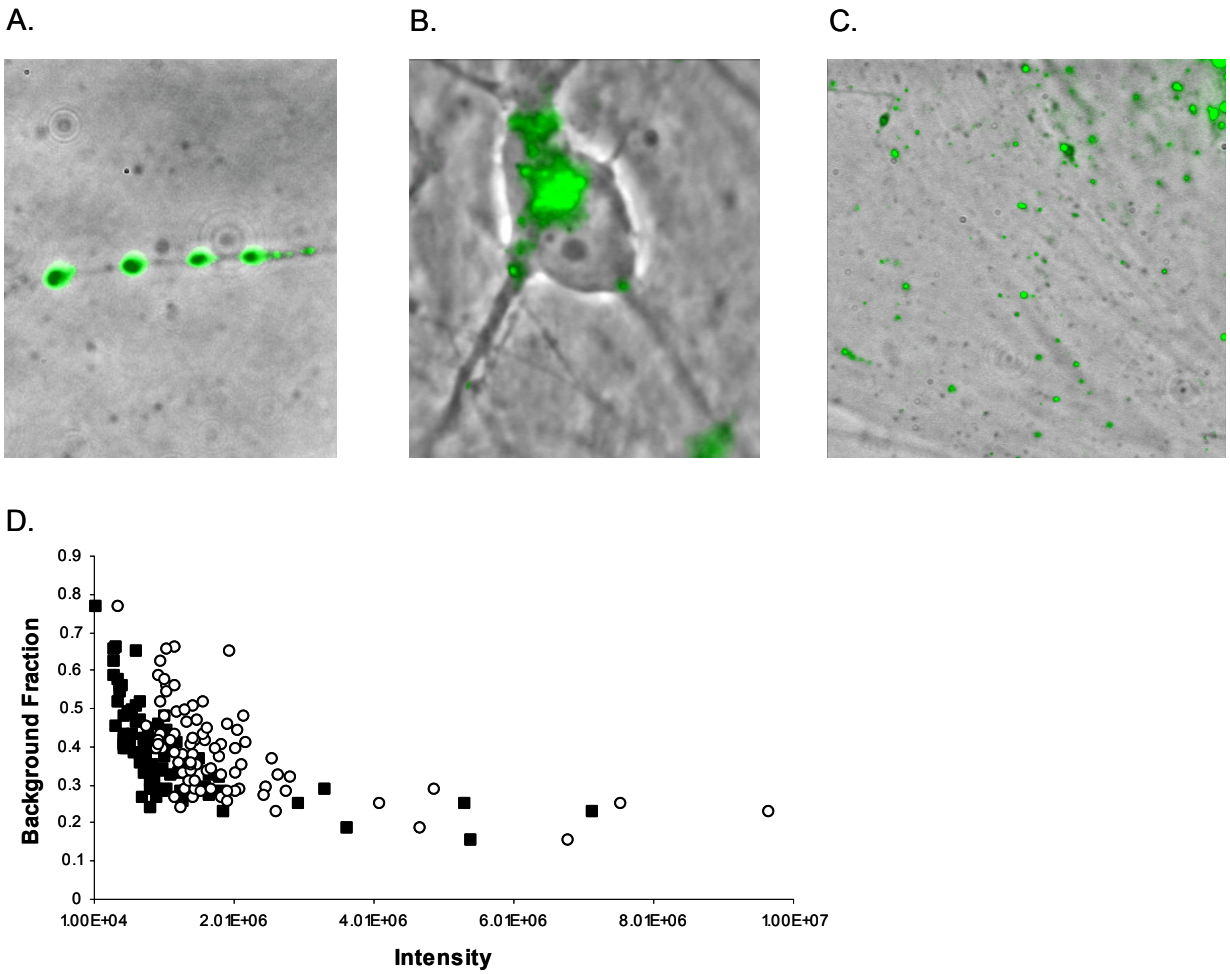

Figure 7 Large bright puncta are functional synapses. Examples of nonspecific labeling that can be eliminated by inspection include: *A*, beading and varicosities in neuronal processes *B*, diffuse labeling within the soma C, vacuoles and vesicles within glia (astrocytes). The labeling in *C* was performed in a purified astrocyte culture for illustration, but similar labeling occurs within the mixed neuronal-glial culture used in our experiments. *D,* The residual background fluorescence remaining after unloading putative synaptic puncta (n = 82) labeled with FM 1-43 is plotted versus the starting (open circles) and unloading (closed squares) intensities. Notice that the fraction of background fluorescence decreases as the initial intensity of the puncta increases, indicating that bright puncta release a larger fraction of their dye upon exocytosis and are indeed functional synapses.

3.2. FCS OBSERVES SLUGGISH VESICLE DYNAMICS

Figure 6D displays the fluorescence intensity from a single synapse as a function of time. Here the number of photons measured during each time bin decays at a modest rate due to photobleaching, and can be corrected after fitting to an exponential function (Fig 6E). In addition to the overall decay of the time trace, one observes intensity fluctuations resulting from putative vesicle motion. The fluorescence intensity autocorrelation function $G(\tau)$, calculated from this time trace is shown in Fig. 6F. As described in section 2.1, $G(\tau)$ quantifies the correlation between intensity fluctuations observed τ seconds apart, which contain information about the underlying vesicle motion.

These measurements were repeated for an ensemble of labeled synapses (n = 39), each with an integration time of T = 200 s. As shown in Fig. 8A, there is a great deal of heterogeneity within the ensemble, particularly in the amplitude of the correlation function G(0) (coefficient of variation $c_{G(0)} = 0.92$). This large variation is not surprising and has been observed in several other measurements in these synapses, such as synapse size and release probability (Dobrunz and Stevens 1997; Murthy, Sejnowski et al. 1997; Schikorski and Stevens 1997). This variation in G(0) may be intrinsic to the population of synapses and may reflect the tuning of some process that is important for synaptic function. Alternatively, the heterogeneity may be the result of experimental noise. To address this issue, the measurement for a subset of these synapses (n = 23) was repeated at a different location (at least one light-box diameter away) within the same synapse. We find that the variation in G(0) within the synapse $\left(\frac{1}{N}\sum_{j=1}^{N}(G(0)_j^{2nd} - G(0)_j^{1st})^2\right)^{1/2}$ is 58% of that between synapses $\left(\frac{N!}{(N-2)!2!}\sum_{j=1}^{N}\sum_{k<j}(G(0)_j^{1st} - G(0)_k^{1st})^2\right)^{1/2}$, indicating that about half of

the heterogeneity is inherent to the population of synapses. The correlation between measurements within the same synapse is demonstrated in Fig. 8D. To examine the average behavior of vesicles in these synapses, the autocorrelation functions from individual boutons were averaged and the result is shown in Fig 8B.

Fluctuations can arise from a variety of instrumental sources, including the laser and the detector. These fluctuations could contribute to the measured synaptic FCS signal. To measure the contribution of instrumental noise to the synaptic G(τ), we repeated the same experiment on cells that were labeled with AM 1-43 and then preserved with the fixative agent paraformaldehyde. Notice that the amplitudes of the fluctuations measured from synapses of fixed (dead) cells are orders of magnitude smaller than those measured in the synapses of live cells. This demonstrates that the signal measured by the synaptic G(τ) is intrinsic to living synapses and is not dominated by instrumental fluctuations.

The correlation time is one important parameter that can be extracted from the autocorrelation function. Our experiments yield an average correlation time of $\tau_{1/2}$ = 2.8±0.4 s, where $G(\tau_{1/2})$ = 1/2G(0). We can gain physical intuition about this number by relating it to a diffusion coefficient and an effective viscosity of the vesicles' surroundings. If we assume that $\tau_{1/2}$ corresponds to a diffusion time $\tau_{1/2} = w^2/D$, then we find an effective diffusion coefficient of D = 4.3±0.7 x 10^{-11} cm^2/s. Assuming that the vesicles diffuse in a medium characterized by a single viscosity coefficient, the Stokes-Einstein relation ($D = k_B T/6\pi a\eta$) yields an effective viscosity η = 25 poises for T = 293 K and the vesicle radius a = 20 nm. This viscosity is 2,500 times larger than water and approximately 100 times larger than expected for inert particles of this size diffusing in the cell (Luby-Phelps, Castle et al. 1987). Accordingly, one of the goals of this thesis is to understand the source of this large correlation time.

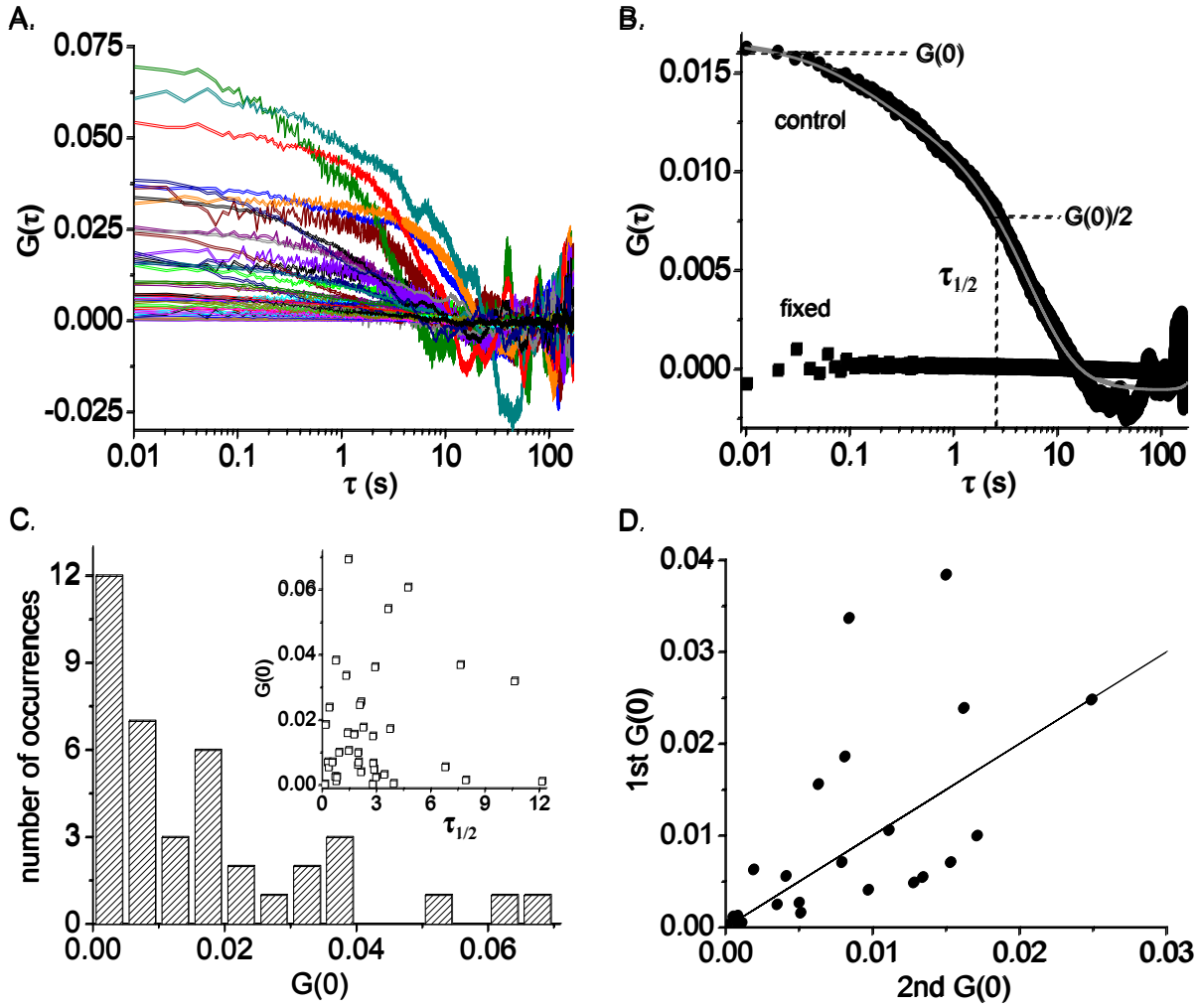

Figure 8 Synapses are heterogeneous. *A*, Ensemble of G(τ)'s measured from n = 39 different synapses. *B*, The average of the correlation functions in *A* is plotted (closed circles) with the amplitude G(0) = 0.016±0.002 and the correlation time $\tau_{1/2}$ = 2.82±0.4 s marked. The gray line represents the fit to the stick-and diffuse model (τ_B = 4.5±1.1 s, τ_U = 2.1±1.5 s, τ_D = 0.19±0.17 s). The closed squares represent the average correlation function for synapses labeled with dye and fixed with paraformaldehyde (n=41). For both the control and the fixed synapses, the error bars are smaller than the points. *C,* A histogram of G(0) from the correlation functions shown in *A*. $\tau_{1/2}$ versus G(0) for each correlation function is plotted in the inset, with little correlation between the parameters. *D*, The spatial heterogeneity was measured by making two FCS measurements spaced at least one light-box diameter away within the same synapse (n=23). The G(0) of the1st measurement is plotted against G(0) of the 2nd measurement, and scatter about the line of slope one.

3.3. RECYLING VESICLES CONSIST OF A MOBILE AND AN IMMOBILE POOL

FRAP measures the mobility of fluorescent objects by monitoring the fluorescence intensity as it recovers within an area previously bleached by an intense laser beam (Schlessinger, Koppel et al. 1976). As discussed earlier, it is more suited for measuring slow dynamics than FCS, and can provide complementary information about mobility and the fraction of mobile particles. We used the experimental setup used in the FCS experiments to measure FRAP of FM 1-43 labeled vesicles within the synapse. Photobleaching destroys fluorescent molecules through the generation of free oxygen radicals that can also destroy cellular components. Therefore, it is important to demonstrate that probing the synapse with FRAP does not destroy its function. Figure 9A shows a labeled synapse before and approximately one minute after a portion of the synapse has been bleached. In addition, the same synapse is displayed after application of high K^+ bath solution. The diminished fluorescence indicates that vesicles within the synapse are still able to undergo exocytosis and that the synapse is still viable after photobleaching. The recovery of an ensemble of synapses and the average recovery are displayed in Fig. 9B and 9C, respectively. Similar to the measurements of G(0), there is significant heterogeneity in the asymptotic level of fluorescence recovery (coefficient of variation c_R = 0.35). The average recovery is about 15%, indicating that a vast majority of labeled vesicles are not mobile and explains why the bleached area in Fig. 9A remains dark (Kraszewski, Daniell et al. 1996). The fluorescence recovery has two identifiable time scales. The fast time scale $\tau_F \approx 4$ s agrees well with the correlation time $\tau_{1/2} = 2.8 \pm 0.4$ s measured by FCS. The slow time scale $\tau_S \approx 40$s is comparable to the total FCS integration time T and is not accessible in those measurements, (see section 2.2).

The amplitude of the correlation function G(0) measured by FCS is the variance of the number of labeled vesicles in the light-box (section 2.1), and is independent of $\tau_{1/2}$ (Fig. 8C). For the average correlation function displayed in Fig. 8B, G(0) = 0.016±0.002. Recall that, the fluctuations of the number of freely diffusing particles in the light-box obey Poisson statistics with the result G(0) = 1/<N>, where <N> is the average number of fluorescently labeled particles in the light-box. However, for a system containing an immobile population, $G(0) = \langle N_M \rangle / \langle N \rangle^2$ (Levene, Korlach et al. 2003), where $\langle N \rangle = \langle N_M \rangle + \langle N_I \rangle + \langle N_B \rangle$ and $\langle N_M \rangle$ and $\langle N_I \rangle$ are the average number of mobile and immobile vesicles respectively in the light-box. $\langle N_B \rangle$ is the amount of background fluorescence in units of vesicles. Measuring the fluorescence remaining in puncta after sustained exocytosis gives $\langle N_B \rangle / \langle N \rangle = 0.3$ (Appendix). We can estimate the average number of vesicles in our light-box ($\langle N_I \rangle + \langle N_M \rangle = 0.7 \langle N \rangle$) by solving the above expression for $\langle N \rangle = (\langle N_M \rangle / \langle N \rangle)/G(0)$, where $\langle N_M \rangle / \langle N \rangle$ can be measured by the asymptotic level of the FRAP curve in Fig. 10C. This level must be adjusted for the total synaptic fluorescence remaining after bleaching, which is 87±2 %. The remaining fluorescence recovers to 16.2±0.9 % on the time scale of the FRAP experiment (~70s), which is comparable to the FCS integration time. Hence, G(0) reflects only a fraction of this recovery, and the above $\langle N_M \rangle / \langle N \rangle$ is an upper bound[3]. This yields $\langle N_I \rangle + \langle N_M \rangle$ to be less than 7±2 labeled vesicles in the light box and less than 60±30 total labeled vesicles in a typical synapse[4]. This is consistent with the majority of studies involving quantal dye uptake (Murthy and Stevens 1999; Harata, Pyle et al. 2001) and counting labeled vesicles with electron microscopy via photoconversion (Harata, Ryan

[3] The FRAP signal recovers to ~10% in $10\tau_{1/2}$ (~30s), which perhaps is a more appropriate value to compare with G(0), but is not rigorous. This value is consistent with the scaling factor for fast refilling considered in the Discussion.

[4] One potential point of confusion is that FCS and FRAP measurement are performed on large synapses and the number of vesicles per light box is derived from those measurements. In contrast, the number of vesicles per synapse is calculated for typical sized synapses. This is valid as long as the density of vesicles remains constant for different sized synapses, which is likely the case (Murthy and Stevens 2001).

et al. 2001), which show that the total number of labeled vesicles in the average synapse is 25 to 30, with one study measuring as many as 120 (Ryan, Reuter et al. 1997). This result confirms that our earlier estimate of the ratio of the synapse to light-box area is reasonable. More importantly, it demonstrates that both G(0) and the asymptotic level of FRAP are small because there exists a large population of immobile recycling vesicles, with $\langle N_I \rangle / (\langle N_I \rangle + \langle N_M \rangle) = 77 \pm 8$ %. If 2/3 of recycling vesicles reside in the reserve pool (Murthy and Stevens 1999) and RRP vesicles remain docked on time scales longer than the experiment (~140 s, (Murthy and Stevens 1999)), then one can conclude that 66% of reserve vesicles are immobile.

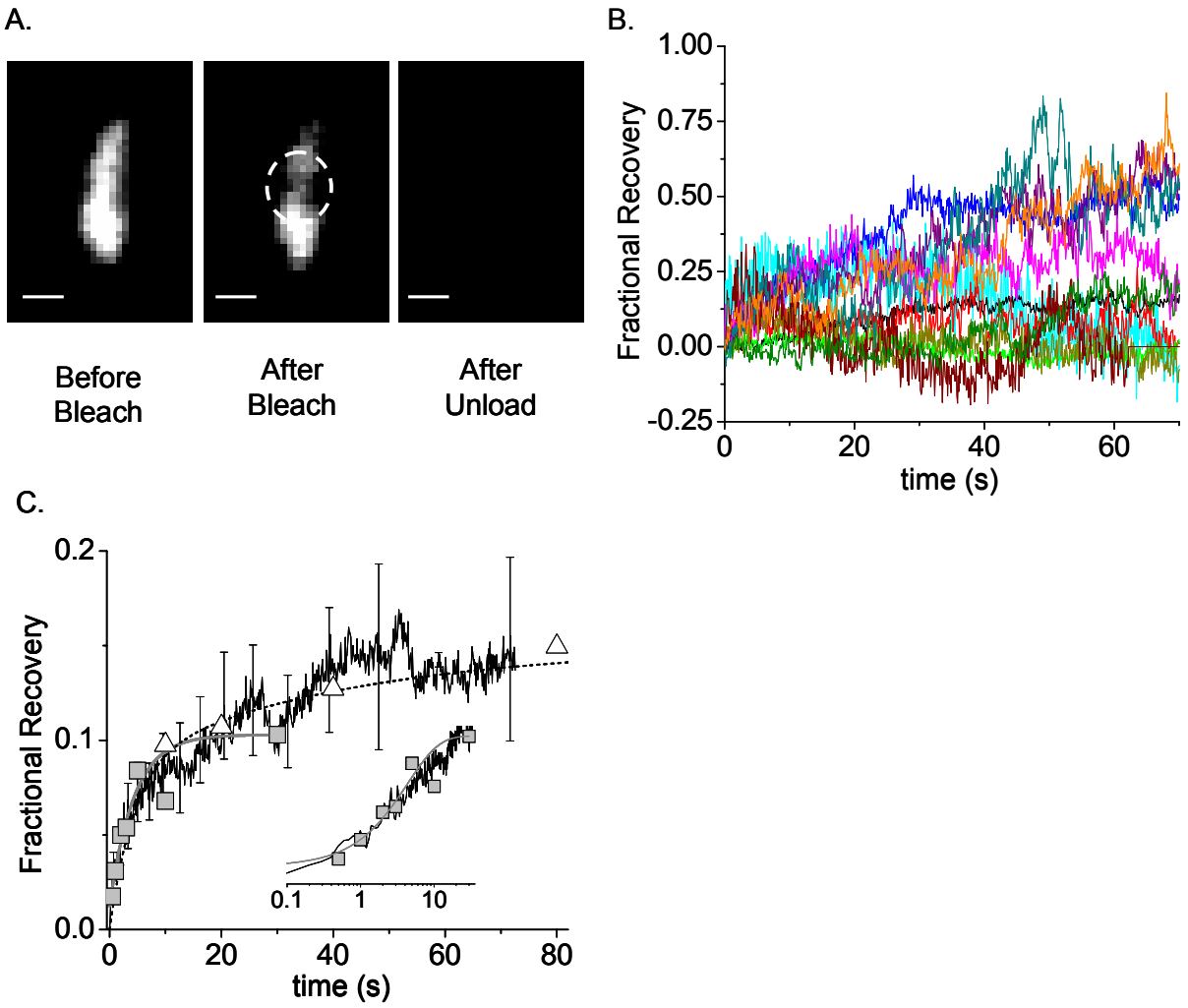

Figure 9 FRAP resembles refilling of RRP. *A*, A synapse labeled with the FM 1-43 is shown before and ~1 min after an area is photo-bleached with a laser. The same synapse is also shown after high K+ bath is applied (scale bar 0.5 μm). *B*, A sampling of FRAP curves (n = 12) randomly chosen from the full ensemble (n = 47). *C*, The average FRAP response of the entire ensemble is plotted with error bars (standard deviation) and is fit to a double exponential (dotted line) $A(f(1-\exp(-t/\tau_F)) + (1-f)(1- \exp(-t/\tau_S)))$ with τ_S = 4 s, τ_F = 40 s, A = 0.15, and f = 0.58. Rescaled refilling data of the RRP measured by Morales et. al. (2000) (closed squares, scaling factor 0.10) and Stevens and Wesseling (1999) (open triangles, scaling factor 0.16) reveal short and long time refilling respectively. The solid gray line is the fit of the simplified stick-and-

diffuse model to the fast refilling experiments with fitting parameters τ_B = 4.32 s and τ_U = 0.59 s. The inset shows the same data on a semilog scale to emphasize early times.

3.4. SYNAPTIC MOTION IS NOT THE SOURCE OF THE OBSERVED DYNAMICS

Synaptic boutons are dynamic structures, whose shape and size evolve with time (Colicos, Collins et al. 2001). Such synaptic motion could contribute to the measurement of fluorescence intensity fluctuations and fluorescence recovery, as the fluorescent synapse moves relative to the fixed laser beam. To determine the contribution of this motion, we used video fluorescence microscopy to track the center of mass position of individual synapses labeled with FM 1-43. Figure 10A shows an example of the trajectory of the center of mass of a synapse and its resulting mean squared displacement $<\Delta r^2(t)>$. Similar to a diffusing particle, $<\Delta r^2(t)>$ grows linear with t. The slope of this line is equal to $4D_{CM}$, where D_{CM} is the effective diffusion coefficient of the center of mass. The trajectory was measured for 30 synapses and the average $<\Delta r^2(t)>$ is plotted in Fig. 3B, with the average diffusion coefficient of the center of mass D_{CM} = 5.4 x 10^{-15} cm^2/s. This motion is ~10 times faster than the intrinsic drift of the experimental setup, which was measured by recording the position as a function of time of 0.42 μm diameter FITC labeled beads (n = 75) adsorbed onto a glass cover-slip (Fig 10B). More importantly, the synaptic D_{CM} is ~8,000 times smaller than that measured for vesicle motion using FCS and ~500 times smaller than for the slow timescale measured by FRAP. Thus, the observed FCS fluctuations and FRAP signal cannot be attributed to any relative motion between the synapse and the laser spot.

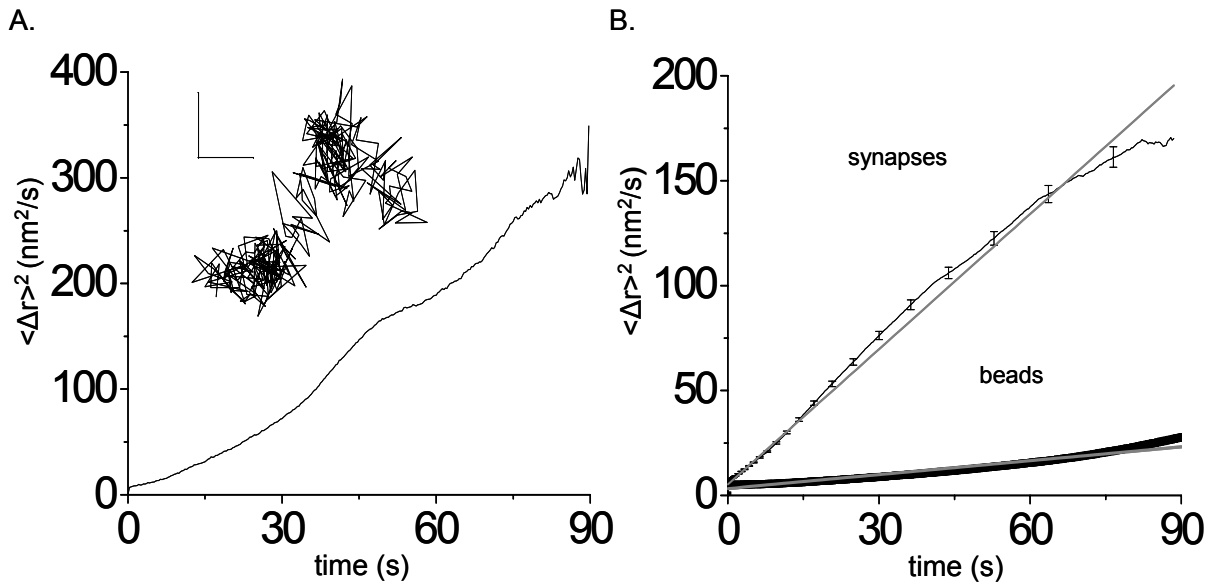

Figure 10 Synapse center of mass motion does contribute to the FCS measurement. *A*, The inset displays the trajectory $\vec{r}(t)$ of the center of mass of a typical synapse. (0.3s/step totaling 90s, scale 5 nm). The mean squared displacement $\left\langle \Delta\vec{r}(t)^2 \right\rangle = \frac{1}{T-t}\int_0^{T-t}[(\vec{r}(t'+t)-\vec{r}(t')]^2\,dt'$ calculated from this synapse's trajectory is plotted below the inset. Here *T* is the total integration time. *B*, The average $\left\langle \Delta\vec{r}(t)^2 \right\rangle$ was calculated for n = 30 synapses and is displayed (top line with error bars) along with a linear fit (gray line) of slope 4D = 2.15 nm^2/s. The average mean square displacement $\left\langle \Delta\vec{r}(t)^2 \right\rangle$ for 0.42 μm fluorescent beads (bottom black line, with the thickness exceeding the error, n = 75) adsorbed to a glass cover-slip is displayed along with a linear fit (gray line) of slope 4D = 0.22 nm^2/s.

4. EXPERIMENTAL RESULTS II: PERTURBATIONS OF VESICLE DYNAMICS

Here we describe several experiments that perturb the motion of vesicles in order to deduce the mechanism underlying their dynamics. These include mechanical and pharmacological perturbations of the synapse.

4.1. VESICLE MOTION IS NOT DUE TO THERMAL FLUCTUATIONS OF THE CYTOMATRIX

The synapse's collection of structural proteins is termed the cytomatrix. This matrix combines with water to form a gel that can behave as a viscoelastic medium inside cells (Howard 2001). As discussed in the section 1.7, there is a body of work that suggests that synaptic vesicles are tethered to this matrix, which is consistent with our finding that the majority of recycling vesicles are immobile. It is also known that viscoelastic media can have slow thermal fluctuations with large effective viscosities that appear similar to diffusion (Tanaka, Hocker et al. 1973). Therefore, it is possible that all the vesicles are tethered, and a few vesicles undergoing thermal fluctuations at the edge of the light box account for the observed low amplitude fluctuations and the slow diffusive-like motion.

To address this question we excited the matrix with mechanical excitations. Viscoelastic media obey the fluctuation dissipation theorem, which predicts that deformations of the gel will relax on a time scale commensurate with the time scale of thermal fluctuations of the system.

This holds because thermal fluctuations excite the same degrees of freedom as small amplitude mechanical deformations of the gel. Thus if the cytomatrix is in thermal equilibrium or close to it, one can probe the timescale for thermal fluctuations of the matrix by measuring the relaxation due to mechanical perturbations. To achieve this, we repeatedly deformed the synapse with a puff (3-4 ms and 4-6 PSI) of extracellular fluid from a glass micropipette placed one to two microns away from the synapse. The forcing is approximated as a square pulse and is cross-correlated with the synaptic fluorescence intensity emanating from the light box. The cross-correlation from a typical experiment is shown in Fig 12. The response to the perturbation relaxes with multiple time scales τ_{slow} and τ_{fast}, which can be modeled with a one dimensional damped harmonic oscillator model (section 3.3). The average cross-correlation from a collection of synapses (n = 13) is displayed in Fig 11B. Notice that τ_{slow} = 29 ms is two orders of magnitude faster than the fluctuations measured by the autocorrelation function of vesicle motion (Fig. 8). Thus, the vesicle motion in resting synapses cannot be explained by thermal viscoelastic fluctuations of the synaptic cytomatrix.

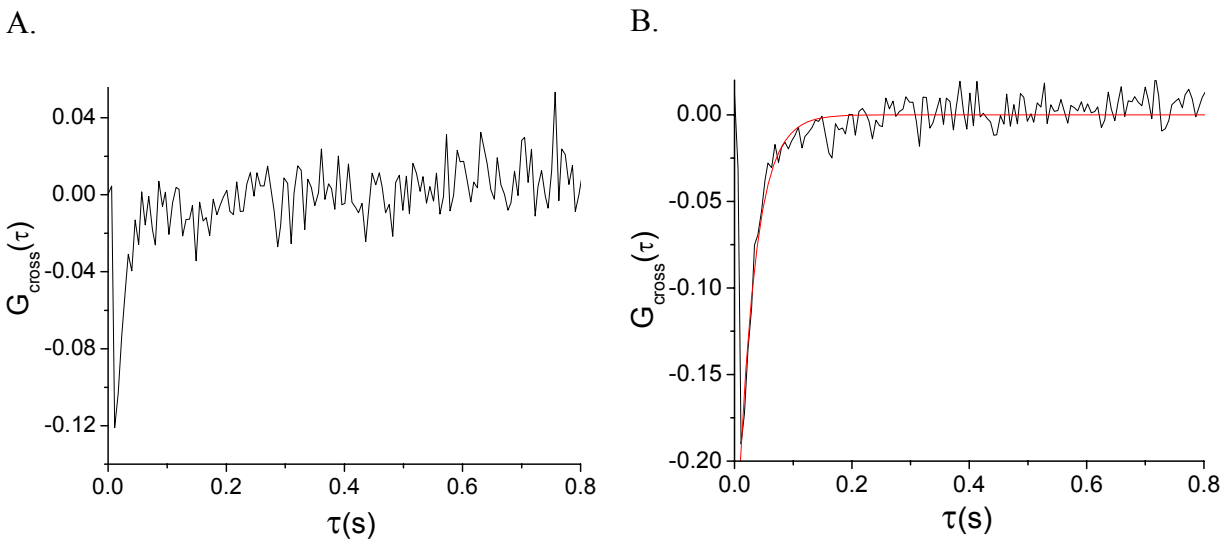

Figure 11 Measured vesicle dynamics are not thermal viscoelastic fluctuations. *A*, Cross-correlation calculated from fluorescence intensity trace from a single bouton exposed to one pressure puff (4ms, 4PSI) applied every 1.5 sec for 150 sec. *B,* Average cross-correlation function calculated from an ensemble of synapses (n=13). The functional fit to a one dimensional damped harmonic oscillator model is shown (section 3.3), with τ_{fast} = 4.5ms and τ_{slow}= 29.5ms.

4.2. PHOSPHORYLATION FREES VESICLES

The phosphatase inhibitor okadaic acid (OA) has been shown to increase the mobility of synaptic vesicles at the neuromuscular junction (Betz and Henkel 1994; Henkel, Simpson et al. 1996), although this phenomenon may not be universal among different synapse types (Guatimosim, Hull et al. 2002). It is thought that this occurs primarily by shifting the population of synapsin proteins to the phosphorylated state, which releases vesicles from the synaptic cytoskeleton (Greengard, Valtorta et al. 1993; Pieribone, Shupliakov et al. 1995; Chieregatti, Ceccaldi et al. 1996). Other studies such as those by Sankaranarayanan et al. (2003) suggest that vesicles in hippocampal synapses bind to other structural proteins rather than actin. Therefore, the stickiness of the synaptic cytoskeleton or other structural proteins may explain the observed slow dynamics of these vesicles.

To explore this idea, we examined the effect of OA on hippocampal synapses labeled with FM 1-43. Images show that OA tends to fade and smear the majority (~90%) of puncta, with the average puncta losing greater than 70% of its vesicles (Fig. 12A). This large value indicates that the application of OA frees vesicles that were previously immobile. We also used FCS to measure the effect of OA on the dynamics of these vesicles. The measurements show that these puncta can be divided into two well-separated groups, sensitive and resistant, based on their correlation times. Resistant puncta are 50% brighter and exhibit dynamics whose decay time is too long for the correlation function to converge. Similar mixed effects of OA treatment have been observed by Betz et. al. (Betz and Henkel 1994) in the neuromuscular junction. In contrast, sensitive puncta are dimmer and exhibit dynamics whose average decay time is $\tau_{1/2}$ = 0.10±0.04 s, which is about 30 times faster than the control synapses. The average correlation

function changes its form significantly and can be described well by free diffusion in a confined geometry (Fig. 5B). This free diffusive motion contrasts to the non-diffusive directed motion observed in the neuromuscular junction (Betz and Henkel 1994) and the impairment of vesicle motion in ribbon synapses (Guatimosim, Hull et al. 2002). The diffusion coefficient for vesicles in hippocampal synapses exposed to OA agree with the diffusion coefficient measured for inert particles of this size in cells (Luby-Phelps, Castle et al. 1987) and for vesicles in ribbon synapses, which lack synapsin (Holt, Cooke et al. 2004). Thus, eliminating the phophorylation dependent binding of RP vesicles to the cytomatrix allows them to diffuse freely.

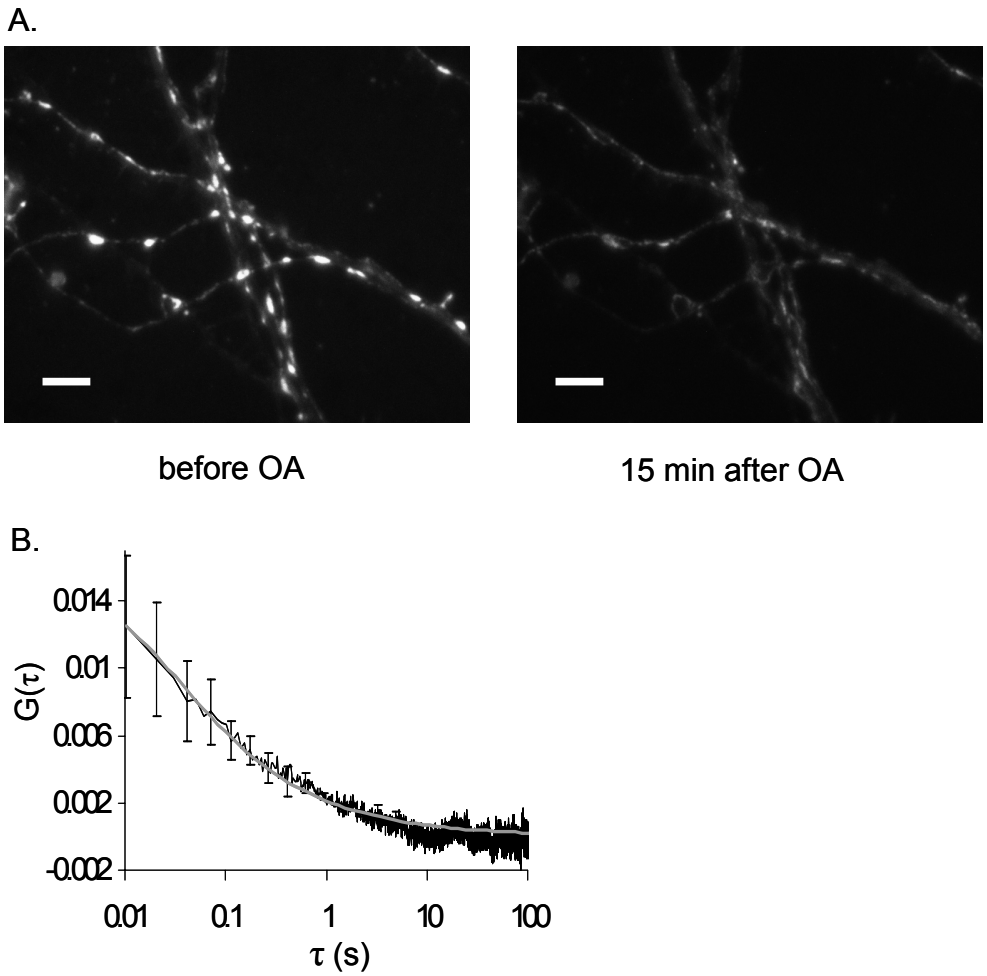

Figure 12: Okadaic Acid (OA) frees vesicles. *A*, Fluorescence image of FM 1-43 labeled synapses before and 15min after continuous application of 2 μM OA (scale bar 5 μm). By measuring the labeling of neuronal processes, one can estimate the nonspecific contribution to the punctas' fluorescence (see section 2.3). The remaining intensity is due to vesicles (~80%). Greater than 70 percent of this vesicular fluorescence is lost to diffusion after 15min in OA. *B*, The average autocorrelation function from OA-sensitive synapses (n=7) is plotted (black line) along with a fit (gray line) to 2D free diffusion with one dimension confined to twice the light-box size (Gennerich and Schild 2000).

4.3. ELIMINATING POLYMERIZED ACTIN DOES NOT FREE VESICLES

Classic experiments show that vesicles bind to actin filaments via synapsin (Greengard, Valtorta et al. 1993; Pieribone, Shupliakov et al. 1995; Chieregatti, Ceccaldi et al. 1996), while more recent measurements in hippocampal cultured neurons find that both the intensity of labeled puncta and the time scale to empty the recycling pool are only slightly altered under conditions that virtually eliminate filamentous synaptic actin (Sankaranarayanan, Atluri et al. 2003). Thus, the role of actin in these synapses remains unclear.

There also exists evidence that the phosphorylation of synapsin not only releases synaptic vesicles, but also depolymerizes actin filaments (Chieregatti, Ceccaldi et al. 1996). Actin is the most abundant structural protein in the synapse, with ~20-30% of it being in the polymerized form within the resting synapse (Sankaranarayanan, Atluri et al. 2003). The actin network largely accounts for the sizeable effective viscosity measured inside of the cell. For example, particles larger than 50 nm are essentially immobile within the cell (Luby-Phelps, Castle et al. 1987). This scale is set by the typical mesh size of the crosslinked actin polymer network (Howard 2001). Synaptic vesicles are 40 nm in diameter, which is near this immobile limit. Could the effects of OA be due to the depolymerization of actin rather than the phosphorylation activated unbinding of vesicles? The distribution of mesh sizes within the polymerized actin network could account for both the sluggish dynamics and the immobile vesicle population. To address this issue we asked two questions: 1) Can OA depolymerize the synaptic actin network? 2) Can depolymerizing the synaptic actin network reproduce effects of OA on vesicle dynamics? To answer the first question we examined the effect of OA on synaptic actin labeled with Green Fluorescent Protein (GFP). Figure 13 shows a fluorescence image, where a subset of the neurons have been transfected with the gene that produces GFP-actin. The puncta represent synapses

where polymerized actin is known to concentrate (Morales, Colicos et al. 2000; Colicos, Collins et al. 2001; Sankaranarayanan, Atluri et al. 2003). Application of the pharmocological agent latrunculin has been shown to depolymerize 97% of synaptic actin (Sankaranarayanan, Atluri et al. 2003) by sequestering actin monomers (Coue, Brenner et al. 1987). Notice that application of latrunculin B (LatB) causes the vast majority of GFP-actin puncta to disappear within a few minutes. In contrast, the addition of OA has little effect on GFP-actin puncta, indicating that the polymerized actin in these synapses remains largely intact (Fig.14B). We should note that from these pictures alone, one cannot distinguish postsynaptic from presynaptic GFP-actin puncta. However, these results hold for virtually all puncta across different fields and experiments.

If the major effect of OA on vesicle dynamics is the depolymerization of actin filaments, then depolymerizing the actin network should reproduce the fast vesicle dynamics seen with OA. To test this idea we examined the effect of LatB on the integrity of FM 1-43 puncta and on vesicle dynamics. Figures 14A show the effect of 20 μM Lat-B on FM 1-43 labeled puncta, showing that the vesicle cluster is largely intact for the first 10 minutes. Unlike, the effects of OA or the effects of Lat-B on GFP-actin, the amount of fading is quite variable among experiments. This fading is not due to photobleaching and is evident after about 10 min. Fading in labeled puncta exposed with Lat-B has been observed previously (Sankaranarayanan, Atluri et al. 2003) and has been attributed to the increase in probability of release that occurs in these synapses upon the depolymerization of actin (Morales, Colicos et al. 2000). FCS experiments on Lat-B exposed synapses show that the form of the correlation function in 60% of these synapses changes dramatically, decaying as $\log(\tau)$ (Fig.14B) Each experiment contained synapses that demonstrated this log behavior as well as those that did not. Although no systematic difference could be identified, between these groups of synapses,

qualitatively healthier cultures appeared to have a larger proportion of the "log synapses". The correlation functions from the remaining synapses have a more familiar diffusive-like form with a longer correlation time. While the form of the correlation function in the log synapses changes dramatically, the correlation time is only slightly altered, with $\tau_{1/2}$ = 1s. This indicates that although eliminating actin filaments has a subtle but measurable effect on vesicles dynamics, it does not result in the free diffusive motion or the substantial decrease in effective viscosity seen with OA. Therefore, it is likely that the phosphorylation alone accounts for the dramatic effect of OA on vesicle dynamics.

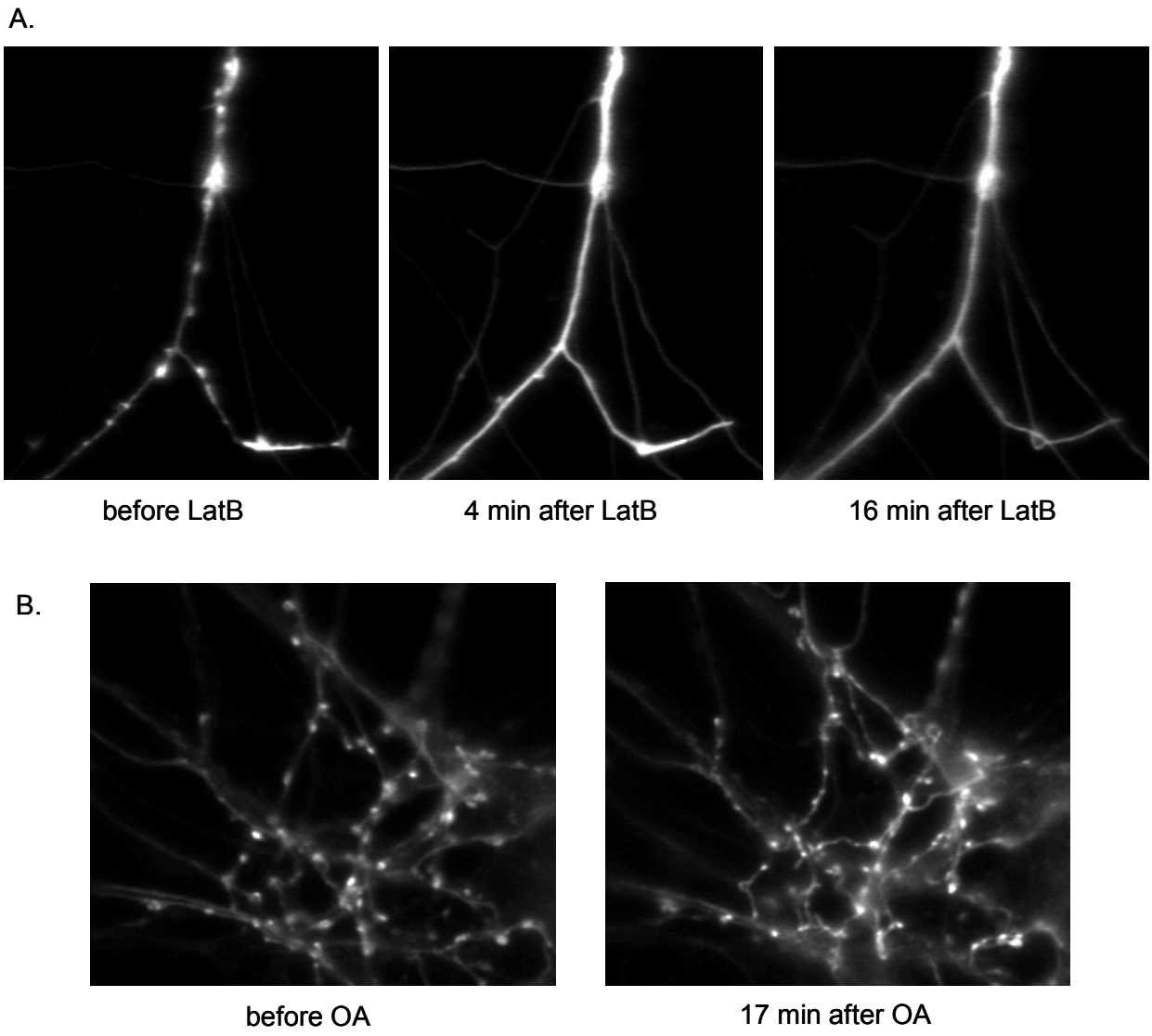

Figure 13 OA does not depolymerize synaptic actin. Fluorescence images of neuronal processes expressing GFP-actin. Puncta represent synapses where polymerized GFP-actin is concentrated. A, Continuous exposure to LatB depolymerizes GFP-actin and eliminates puncta. B, In contrast, continuous exposure to OA leaves GFP-actin puncta intact.

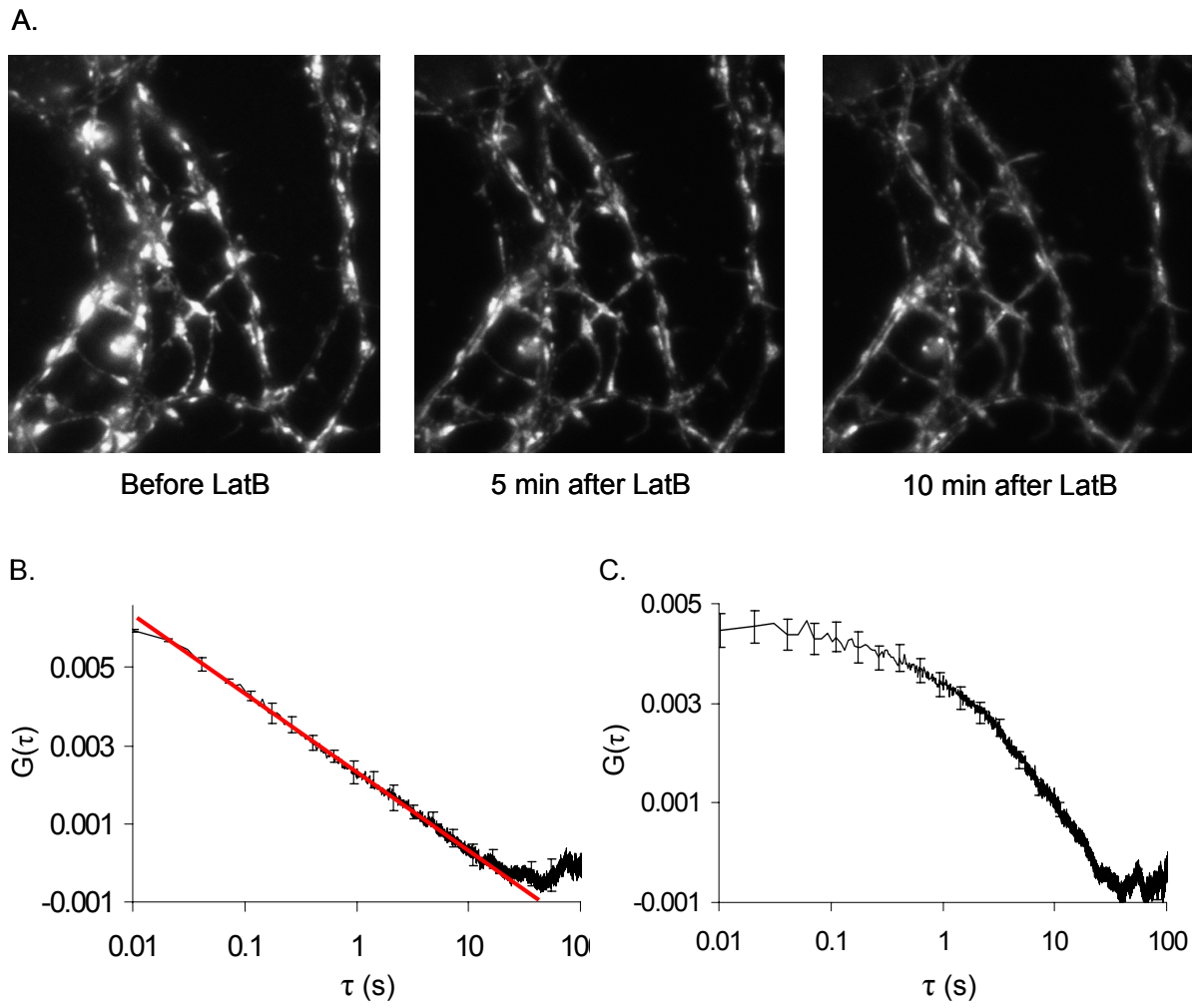

Figure 14 Depolymerizing synaptic actin does not lead to free vesicle diffusion. *A*, Fluorescent images of puncta labeled with FM 1-43 before and after continuous exposure to LatB. FM 1-43 puncta are still intact minutes after the synaptic actin network has been depolymerized. Fading often becomes evident after 10 to 15 minutes. *B*, 60 % of puncta (n = 25) show marked changes in their correlation function, with G(τ) decaying as log(τ), while *C*, the remaining puncta (n = 16) decay with dynamics similar to control synapses.

5. DISCUSSION

5.1. WHAT IS THE EVIDENCE THAT WE ARE MEASURING VESICLE MOTION?

Our experiments suggest that the motion of synaptic vesicles can be measured with FRAP and FCS in cultured hippocampal neurons, at the level of single synaptic boutons, despite their small size. The small G(0) measured by FCS and the slight asymptotic recovery measured independently by FRAP are both consistent with the picture that a large fraction of recycling vesicles are immobile. Together these quantitative measurements provide an estimate for the number of labeled vesicles in the light-box and the synapse, which agrees with previous measurements using fluorescence and electron microscopy in these synapses (Ryan, Reuter et al. 1997; Murthy and Stevens 1999; Harata, Pyle et al. 2001; Harata, Ryan et al. 2001). Also, results from both techniques indicate that mobile vesicles take on the order of seconds or longer to move across the synapse. Control FCS experiments performed on labeled vesicles in synapses of fixed cells indicate that this motion is intrinsic to living synapses, and that the FCS signal in live synapses is not due to fluctuations in laser intensity or other instrument noise. Further, vesicle dynamics in synapses is about three orders of magnitude faster than synaptic motion and mechanical drift measured by video fluorescence microscopy. Finally, the time scale of vesicle dynamics agrees with the time required to refill the readily releasable pool, which we discuss in detail below. These facts strongly imply that we are indeed measuring the dynamics of synaptic vesicles.

5.2. WHY IS VESISCLE MOTION INCONSISTENT WITH FREE DIFFUSION?

Several results lead us to believe that the observed slow vesicle motion is not free diffusion. First, the effective diffusion coefficient for vesicle motion is 100 times smaller than measured for inert particles of the same size diffusing in cells (Luby-Phelps, Castle et al. 1987). Also, the motion of synaptic vesicles is altered significantly by the application of the phosphatase inhibitor OA, which results in vesicles diffusing freely with an apparent diffusion coefficient that is 30 times larger than control synapses. This effect of OA cannot be attributed to the depolymerization of actin filaments. Lastly, eliminating the network of actin filaments with LatB, does not dramatically lower the effective viscosity as would be expected for particles undergoing free diffusion. We compared the experimental correlation function to the correlation function predicted for one and two dimensional diffusion, as well as free diffusion in confined geometries (Gennerich and Schild 2000). In all cases the fits were marginal (Fig. 16 A). Hence, phosphorylation-dependent vesicle binding to unknown proteins within the synaptic cytomatrix is likely the source of the sluggish dynamics, and normal vesicle motion is not simply free diffusion.

5.3. VESICLES UNDERGO STICK-AND-DIFFUSE DYNAMICS

Motivated by our experimental results and the body of work on synapsin (Benfenati, Valtorta et al. 1991; Greengard, Valtorta et al. 1993; Pieribone, Shupliakov et al. 1995), Chuck Yeung constructed a model of diffusing vesicles that stochastically bind to and release from the synaptic cytomatrix via a Poisson process (Fig. 16 B). When the vesicles are unbound they are free to

diffuse with a diffusion constant D so that the characteristic diffusion time over the light-box is $\tau_D = w^2/D$. In the free state, vesicles become bound at a rate $1/\tau_U$. Once bound, the vesicles become free again with an unbinding rate $1/\tau_B$. Therefore, the unbound and bound states last for an average time τ_U and τ_B respectively. This model can be solved analytically, allowing $G(\tau)$ to be calculated. Figure 8B and 16A shows that the fit of the stick-and-diffuse model to the FCS data is quite good with the fitting parameters $\tau_B = 4.5\pm1.1$ s, $\tau_U = 2.1\pm1.5$ s, and $\tau_D = 0.19\pm0.17$ s.

Therefore, our picture of vesicle dynamics is as follows. The majority of recycling vesicles are immobile, and even mobile vesicles spend approximately 70% ($\tau_B/(\tau_U+\tau_B)$) of their time bound. When bound, these vesicles remain stuck for an average time of about 5 seconds. Once unbound, the vesicles are free to move about the bouton becoming bound again after an average time of about 2 seconds. Since $\tau_U/\tau_D \approx 10$, the vesicles can visit an area much larger than the light-box while free. This area corresponds approximately to the area of a typical bouton. Note that the fit of the model to the experimental autocorrelation function is sensitive to τ_U and τ_B, but insensitive to τ_D as long as $\tau_D << \tau_U$. In fact, models differing in the details of the dynamics of the vesicles in their free state would produce comparable fits, as long as the vesicles move fast enough such that the area that they visit while free is much larger than the light-box. Despite the large uncertainty in τ_D, the free diffusion time obtained in our fits is consistent with the diffusion time measured in the presence of okadaic acid ($\tau_{1/2} = 0.10\pm0.04$ s).

Although mobile vesicles spend a majority of their time bound, it is important to make a distinction between mobile vesicles that bind transiently and vesicles that reside in the immobile pool. Since the sticking time τ_B is much smaller than the integration time, these mobile vesicles contribute to both G(0) and the amount of fluorescent recovery after photobleaching. In contrast, the immobile pool of vesicles remain bound on timescales of order of, or larger, than the duration

of the FCS and FRAP experiments. Thus, the immobile pool is a long-lived state compared to the transient binding of the mobile vesicles, and the small G(0) and incomplete fluorescence recovery can only be explained by the existence of two distinct vesicle populations. Immobile vesicles have been observed in these (Kraszewski, Daniell et al. 1996) and in other synapses (Henkel, Simpson et al. 1996; Burke, Han et al. 1997), and are perhaps a universal feature of the vesicle cycle.

5.4. MOBILIZATION OF VESICLES IS THE RATE LIMITING STEP IN REFILLING

As discussed in the introduction, refilling experiments monitor the recovery of exocytosis, after the entire readily releasable (docked) pool of vesicles has fused. Although other mechanisms have been proposed (Pyle, Kavalali et al. 2000), this empirical observation is hypothesized to reflect the mobilization of RP vesicles to the active zone (Rosenmund and Stevens 1996). The majority of studies show that the refilling process can be fit by a single exponential with a relaxation time of 3-10 s. This agrees with the typical correlation time $\tau_{1/2}$ = 2.8 s and the fast fluorescence recovery time $\tau_F \approx 4$ s measured in our experiments. This agreement suggests that vesicle movement to the active zone might be the rate limiting step in refilling. If this is true, then this movement alone should be able to explain the exponential recovery. Figure 9C shows refilling data measured by Morales et al. (2000) that has been rescaled to overlie the averaged data from the FRAP experiments. We see that the refilling of the RRP follows an identical time course as the fast (τ_F) recovery of fluorescent vesicles into the light-box. Next we asked if the fast FRAP and refilling data could be explained by the stick-and-diffuse dynamics used to model the FCS experiments. To simplify the analysis we set $\tau_D = 0$, since the diffusion time is an order

of magnitude faster than the other time scales. At t = 0, a fraction F = $\tau_U/(\tau_U+\tau_B)$ of mobile vesicles are free. Additional vesicles continue to unbind in an average time τ_B. Once free the vesicles diffuse, and because τ_D = 0, distribute instantaneously with uniform probability throughout the synapse. Hence the time for refilling the light-box or the active zone, approximated as a perfect sink (Murthy and Stevens 1999), is determined solely by τ_B, and has the form $(1-F\cdot\exp(-t/\tau_B))$. The fit of the simplified stick-and-diffuse model to the refilling data is shown in Fig. 9C. A separate fit for the FRAP experiment was not done since the refilling and FRAP data coincide. Despite the simplification of the model, the parameters optimized to fit the refilling and FRAP experiments (τ_B = 4.32 s, τ_U = 0.59 s) agree reasonably well with those optimized independently to fit the FCS measurements (τ_B = 4.5±1.1 s, τ_U = 2.1±1.5 s). Much of the discrepancy in τ_U is due to the fact that both the refilling and FRAP data must pass through the origin, while the simplified stick-and-diffuse model cannot due to the infinite diffusion constant. Thus, fitting the simplified stick-and-diffuse model to the refilling data underestimates τ_U, allowing the model fit to approach the origin. Thus, the stick-and-diffuse model of synaptic vesicle dynamics is consistent with both FCS and FRAP results, as well as the previously observed refilling of the RRP.

In contrast to the fast refilling described above, the RRP recovers more slowly after extensive exocytosis (Liu and Tsien 1995; Stevens and Wesseling 1999). This is thought to be a form of synaptic depression whose mechanism is unknown, although several mechanisms, including vesicle mobilization, have been suggested (Pyle, Kavalali et al. 2000). In addition to fast refilling, Fig. 9C also shows rescaled data measured by Stevens and Wesseling (1999) for the refilling of the RRP after depression was induced with 150 action potentials at 9Hz. The slow

component (τ_S) of the FRAP signal matches the slow recovery of the RRP after the sustained activity[5]. Therefore, the slow recovery of the RRP is consistent with the mobilization of vesicles.

One possible mechanism for the slow synaptic depression is that after extensive exocytosis the refilling of the RRP is limited by immobile vesicles joining the mobile pool. The slow refilling is not seen in the fast refilling experiments because the brief application of hypertonic solution only depletes the RRP. In contrast, sustained electrical activity depletes both the RRP and the mobile pool faster than they can be replenished by the immobile pool, resulting in usual depletion, but with slower recovery. Hence, the slow time scale for refilling appears only after both the docked and the mobile pools undergo exocytosis. In contrast, our experiments do not rely on exocytosis, allowing us to observe vesicle mobilization more directly. We conjecture that immobile vesicles become free at minimal levels in resting synapses, and that this process manifests as the slow (τ_S) fluorescence recovery measured in our experiments. If the limited availability of immobile vesicles is truly responsible for the slow recovery of the RRP, then this process is likely to be a key regulatory point in the vesicle cycle (Burke, Han et al. 1997). This idea is consistent with experiments that show that OA frees immobile vesicles, suggesting that the size of the immobile pool is regulated by phosphorylation. Clearly, additional experiments are necessary to address these issues.

[5] Experiments that measure both the fast and slow component of refilling simultaneously (Stevens and Wesseling, 1999) also fit the average FRAP data well (data not shown).

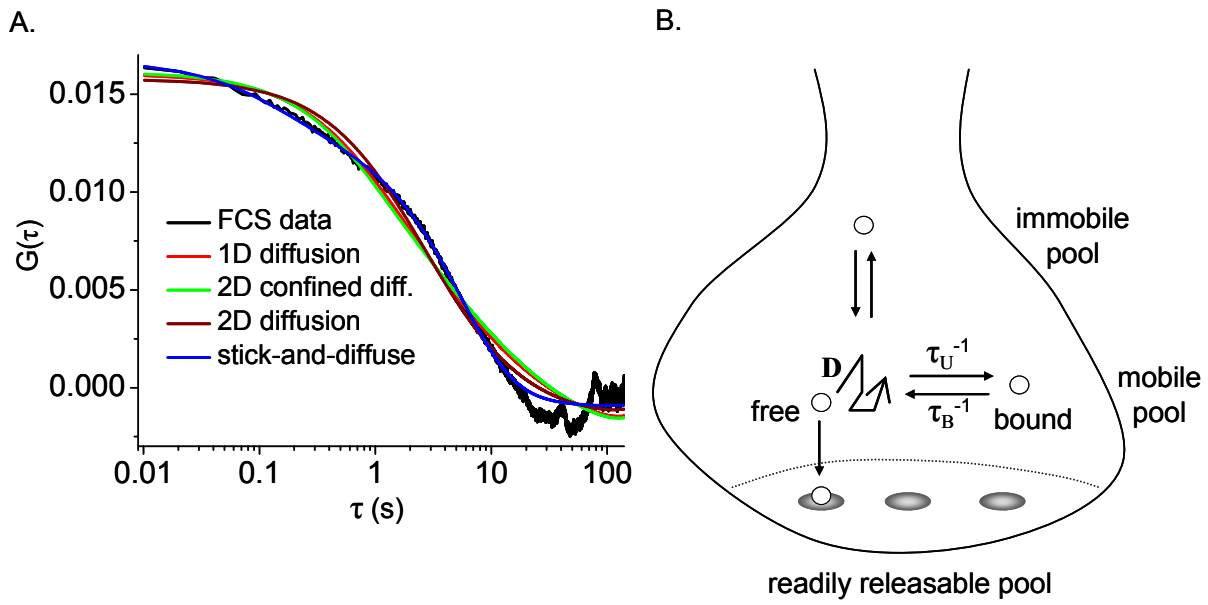

Figure 15 Refilling of RRP is modeled by stick-and-diffuse dynamics. *A*, Compared to the stick-and-diffuse model (blue line), the fit of FCS data to free diffusion is marginal. The average correlation function shown in Fig. 8B is replotted (black trace) along with fits to free diffusion models in one (red line) and two (brown line) dimensions, with diffusion times of τ_D = 1.1 and τ_D = 2.7 respectively. The fit to 2D free diffusion with one dimension confined to twice the light-box size (Gennerich and Schild 2000) is also shown (green line), and overlies the 1D fit. However, for confined diffusion τ_D = 2.0, which is slightly closer to the 2D diffusion constant. *B*, A schematic of the stick-and-diffuse model depicts mobile vesicles stochastically alternating between a bound and a free state. Bound vesicles become free at a rate τ_B^{-1}, the inverse of the average time they remain stuck. Free vesicles diffuse with a diffusion coefficient D, and become stuck at a rate τ_U^{-1}. In addition to mobile vesicles that undergo stick-and-diffuse dynamics, there exists an immobile pool of vesicles, which remains bound on time scales much longer than the transient binding times of the mobile pool. Refilling of the readily releasable pool can be modeled by including docking sites that act as perfect sinks.

5.5. WHY HAS THIS MECHANISM OF VESICLE MOBILIZATION EVOLVED?

The small synapses that dominate the central nervous system have active zones that contain only a few vesicles. As discussed earlier, the number of these vesicles in the RRP determines the probability of release of neurotransmitter. The initial release probability is typically less than 0.5 and diminishes quickly by an order of magnitude with activity. This decrease in probability results from a mismatch between the supply and demand of release competent vesicles. Despite this mismatch, our work suggests that the cell's machinery is built to hinder rather than accelerate the movement of vesicles to the active zone. Why has synaptic transmission evolved to be so unreliable, particularly during times of increased neuronal excitation when information is actively being processed?

One common but unsatisfying answer is that the reliability of synaptic transmission is compromised in order to maximize synaptic density. Achieving dense synaptic connectivity requires minimizing synaptic volume (~0.1μm^3), which places severe constraints on the supply of vesicles. Thus, the brain overcomes the unreliable transmission that results by averaging over many synapses that transmit redundant information (Allen and Stevens 1994; Stevens 1994). There are several reasons to believe that this view is not likely. First, the reliability of synaptic transmission, the number of both docked and total vesicles, and the synaptic bouton volume all scale linearly with each other (Murthy, Schikorski et al. 2001; Schikorski and Stevens 2001). Therefore, doubling the number of boutons for a given neuron in order to double its overall reliability of transmission is equivalent to doubling the size of each of its boutons. The latter strategy is likely to be more efficient, because synapses have certain fixed energetic costs that do not scale with size. For example, each bouton regardless of its size, contains one mitochondria which must be assembled and transported from the soma. Next, unlike the bouton of the

neuromuscular junction where vesicles are close-packed (Rizzoli and Betz 2004), the volume fraction of vesicles in hippocampal synapses is only about 6 % (Schikorski and Stevens 1997), and only 15 % of these vesicles label with FM 1-43 and participate in recycling. It appears that small central synapses have room to increase the size of the recycling pool and hence the rate of steady state neurotransmitter release (section 1.3), but do not utilize this capacity. Therefore, the unreliability of synaptic transmission may have evolved due to a selective advantage rather than as a consequence of a constraint such as bouton size. Consistent with this idea several proteins have been found to impede docking and priming steps necessary for exocytosis including actin, munc18, and synaptophysin (Sudhof 1995; Morales, Colicos et al. 2000).

What advantage could unreliable synapses bestow upon the brain? As mentioned in the introduction, the strength or efficacy of synaptic transmission can be modulated on time scales of milliseconds to hours, and even longer via a set of process collectively termed synaptic plasticity (Abbott and Regehr 2004). The mechanisms underlying this process are actively being investigated and several presynaptic and postsynaptic mechanisms have been implicated (Kandel 2001). However, tuning the probability of release is likely the most sensitive control parameter for synaptic strength (Koch 1999). The large heterogeneity observed in release probabilities (Dobrunz and Stevens 1997) and vesicle motion (Fig 8) among synapses may reflect the tuning of synaptic strength by network activity. To achieve this, the majority of synapses must be unreliable in order to take advantage of the available dynamic range (Goda and Sudhof 1997). Since the probability of neurotransmitter release during activity is limited by the number of recycling vesicles and the time required for them to recycle, the vesicle cycle is likely to be a highly regulated process intimately involved in synaptic plasticity. This is particularly true of rate limiting steps such as vesicle translocation to the active zone. Hence, vesicle immobility and

binding may have evolved to act as brake mechanism to control vesicles' mobilization to the active zone, and to regulate the efficacy of synaptic transmission. Similar brake mechanisms exist throughout the vesicle cycle, from the inactivity of the resting pool to the inhibition of exocytosis of the RRP. This appears to be a common strategy of presynaptic plasticity, which not only explains why multiple vesicle pools exist but also how synaptic strength can be modulated on a variety of time scales.

APPENDIX

A. FCS DETECTION VOLUME IS A SMALL PORTION OF THE SYNAPTIC BOUTON

The area of the light-box is approximately 10 times smaller than that of the synapse, suggesting that the FCS measurement observes a small fraction of the total labeled vesicles in the synapse. To confirm this, we calibrated the mean intensity measured by the avalanche photo-diode (APD) during the FCS experiment against the total fluorescence of FM 1-43 labeled puncta. This dc intensity measured by the APD should represent a small fraction of the total fluorescence emanating from the labeled synapse. To measure the total fluorescence intensity, synapses were loaded with FM 1-43 using the same protocol as used in the FCS experiments. The FM 1-43 loaded synapses were illuminated with a Xenon arc lamp and an image (Fig. 17A) was taken with a camera mounted in the front port of the microscope with a specified gain and exposure time. The synapses were unloaded by perfusing the coverslip three times with high K+ solution without dye, and a second image (Fig. 17B) was taken using the same settings. The two images were aligned and a 1.0 μm circular ROI was drawn around each puncta. The total intensity and the difference intensity for each ROI was calculated, and was repeated for multiple experiments (n = 82 puncta). The histograms for both the starting and difference (unloaded) intensities are displayed in Fig. 17D and Fig. 17E respectively. The mean starting and difference intensities are 2.8 and 1.9 million counts per second respectively. Thus, ~30% of the punctas' fluorescence is not released and this value is used to estimate the nonspecific background labeling.

The intensities of these puncta measured by the camera in the front port could then be calibrated against FCS intensities measured by the APD in the side port of the microscope. This calibration actually involves calibrating two sets of instruments; the APD and the laser used in the FCS experiment against the lamp and the camera used in the above unloading experiment. We describe these calibrations below.

First, we calibrate the 16-bit scale of the camera against the photons counted by the APD. Since intensity is the number of photons per area per second, we must find the area over which the APD together with the pinhole integrate the incoming photons (under wide field illumination). Formally, the pinhole in front of the APD convolves the image that the APD detects. Similarly, we must convolve the image that the camera detects with a window function W in order to properly calibrate the intensities. To measure this window function, we imaged sub-resolution 40nm fluorescent beads illuminated with the arc lamp. This image of sub-resolution beads reveals the point spread function (PSF) of the optical system. The image of individual beads were projected into the side port and scanned across the pinhole and APD at a known velocity (0.3125 um/s). Several of these line scans (Fig. 18A) were averaged to give I_{APD} (Fig. 18C). Likewise images of the beads from the same coverslip and with the same illumination were imaged by the camera mounted in the front port. Line scans along a single row of pixels though the middle of the beads (Fig. 18B) were averaged to give the PSF displayed in Fig. 18C. Notice that in Fig. 18C that the camera's line scan along a row of pixels (PSF) is narrower than the line scan measured by the APD. This is due to the fact that the camera is measuring the PSF of the microscope, while the APD is measuring the PSF convolved by some window function. To mimic the effect of the pinhole we convolve the line scan measured by the

camera (PSF*)* with a square window function *W* of various sizes *d* until it matches the line scan measured by the APD (Fig. 18C).

$$I_{APD}(x) = \int W(x - x')PSF(x')dx' ,$$

where $W(x - x') = 1$ for $|x - x'| \leq d/2$ and 0 otherwise. Notice that as the window size increases, the convolved PSF spreads out and approaches the line scan measured by the APD, with the best match being a window around 5.5 pixels or 440 nm measured in the object plane. When one applies the magnification of the side port of 80x, one finds a window of 35 μm. This agrees well with physical size of the pinhole, which is 50 μm.

To calibrate the counts measured by the camera into photons measured by the APD we labeled a dendrite with FM 1-43 and illuminated it with the same arc lamp as above. The dendrite's image was both captured by the camera (Fig. 19A) in the front port and scanned across the pinhole and APD in the side port (open squares Fig. 19C). The position of the pinhole in reference to the camera image is measured by illuminating the sample with the laser spot, which the pinhole has been aligned to, and taking an image with the camera (Fig. 19B). A line scan in the x direction along the pixels of the camera image was then convolved by a two dimensional 5.5 x 5.5 pixel square window. This convolution integrates the intensity in the square window as it moves along the image and is meant to mimic the pinhole being scanned across the dendrite. The convolved line scan along the camera image (solid squares) as well as the scan across the APD and pinhole (open squares) are displayed in Fig. 19C. After rescaling, the two curves collapse onto each other, reaffirming the correct choice of the window function used in the convolution. The result of the rescaling is that one photon measured by the APD in the side port is equivalent to 39 counts measured by the camera in the front port (on a 16-bit scale at the given camera settings).

We examined whether this number is comparable to the manufacturer's specifications for the camera. The full well capacity of the camera is 400,000 electrons. At the selected settings, the gain is ~375 and the quantum efficiency is ~90% in the dye's spectral range. Thus, at these settings the theoretical number of photons per pixel necessary to saturate the camera is:

$$400{,}000e^{-} / fullwell \div 375 \div .90e^{-} / photon = 1185 photons / fullwell$$

According to the above calibration, each count on the camera in the front port gives 1/39 = 2.57 x 10^{-2} photons measured by the APD in the side port. The APD has a quantum efficiency of ~50%. Also, due to the beam-splitters used to direct light to the various ports, only 80% of the light that the side port sees can reach the front port. Therefore, one count measured by camera is actually 4.11 x 10^{-2} photons. After, you subtract the digitizer offset (1528), the 16bit scale saturates at 64,008. So according to our measurement the camera saturates at:

$$64{,}008 counts / fullwell \times 4.11x10^{-2} photons / count = 2631 photons / fullwell$$

Our calibration agrees within a factor of approximately 2 of the theoretical expectation.

Now we can express the total counts in the labeling experiment shown in Fig. 17 in terms of photons collected by the APD per unit time. If we multiply 1/39 photons per count by the average total fluorescence emanating from the synapse during 1 second, we can get the number of photons per second that the APD would measure with the same illumination. For the fully labeled synapse this would be 72.2 x 10^{3} photons/sec.

The last step is to calibrate the different excitation sources, laser and xenon arc lamp used in the two experiments. To do this we scan the same dendrite in the same location as above with a laser intensity typically used in the FCS measurements (~0.005μW) and measure the

fluorescence intensity. This can be directly compared to the analogous scan of the dendrite illuminated by the arc lamp described above. Both are scanned in the same manner and measured with the same APD and pinhole. The scan of the dendrite with the laser is plotted (open circles) in Fig. 19C. Notice that the profile of the dendrite is narrower when excited with the laser than with the lamp. This improved resolution is a well-known effect in laser confocal microscopy. The fluorescence emitted (as detected by the pinhole and APD) via laser excitation is ~4.5 times greater than that of the lamp. Therefore, a fully labeled synapse excited entirely by the laser would yield approximately 320 KHz measured by the APD.

Finally, we can compare the dc intensity in our FCS experiment with the total fluorescence emanating from the synapse. We use laser intensities from ~0.0025μW to ~0.01μW. Therefore, if the entire synapse was contained within the light-box of the FCS experiment, the dc intensity would lie between 160KHz to 640KHz. Counting rates in our measurement are between 5-70KHz. This is about an order of magnitude smaller than the synapse's total fluorescence, and agrees with ratio of the light-box to the synapse size.

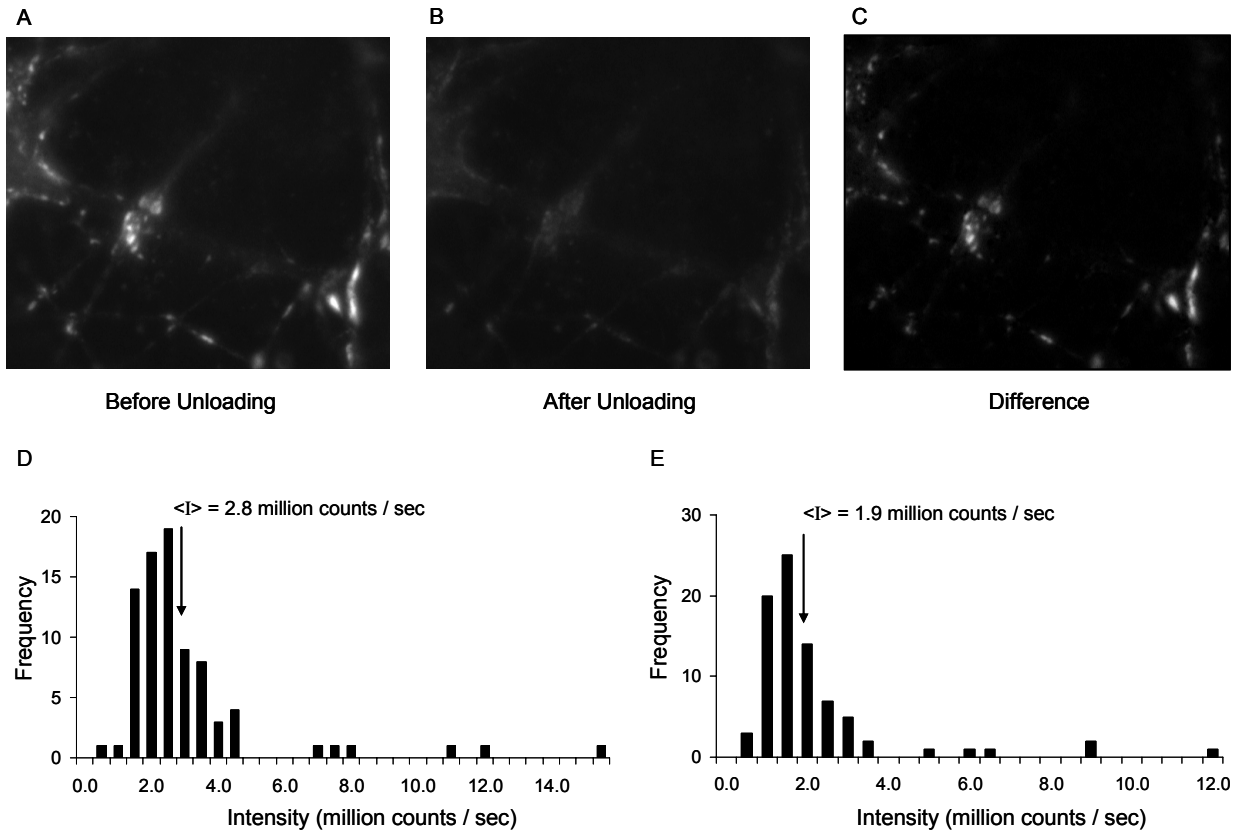

Figure 16 The total fluorescence of FM 1-43 labeled synapses. Image of a field of FM 1-43 labeled puncta (n =82) before (A) and after (*B)* unloading with 3 rounds of high K+ bath solution. *C*, The difference image of *B* subtracted from *A*. Identical ROIs were drawn around puncta in A and B, and the total intensity was calculated for each ROI. *D*, A histogram of the starting intensities for three experiments are displayed in counts on the CCD camera (16-bits per pixel) per second. *E*, A histogram of the difference intensities for the same experiments.

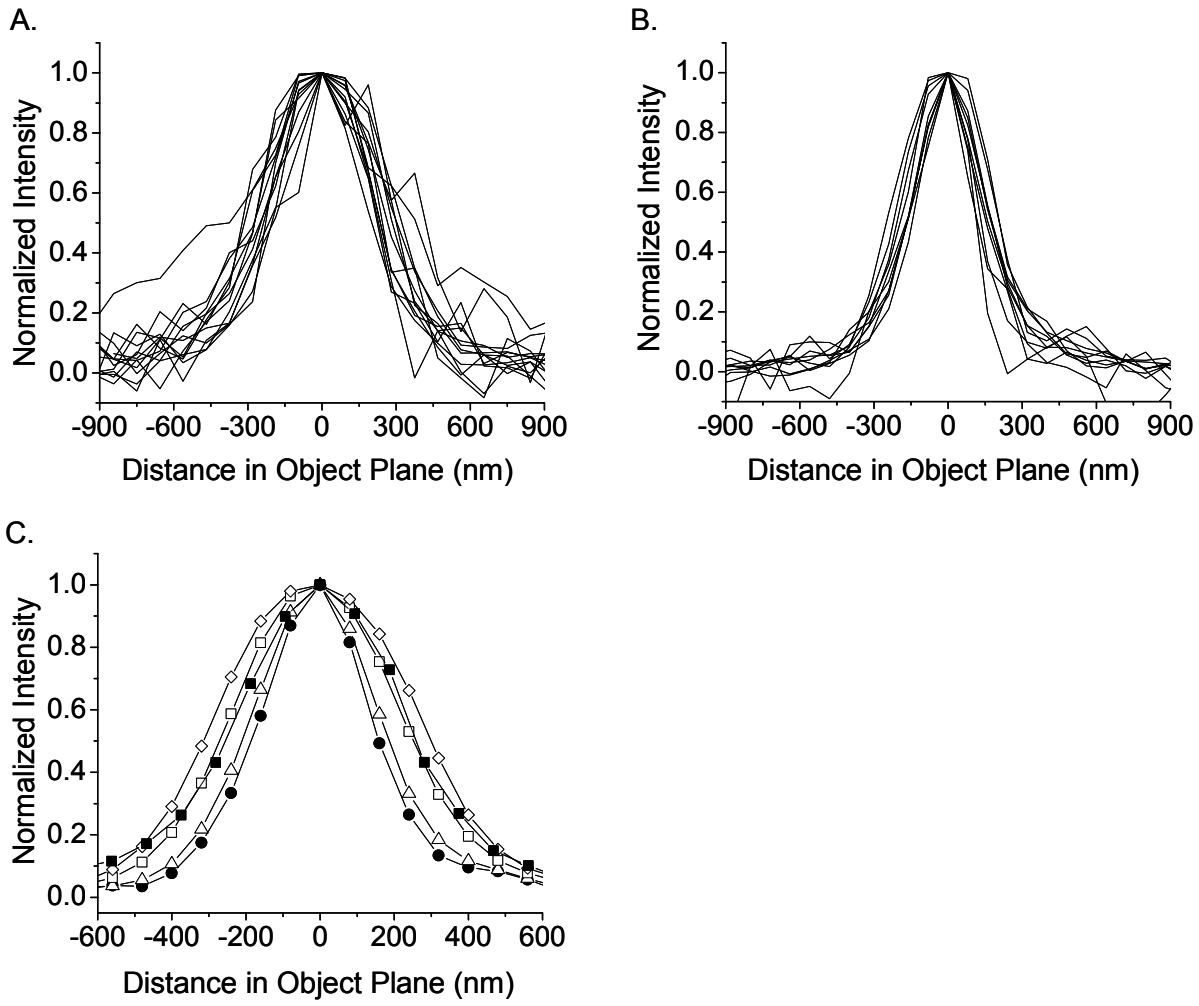

Figure 17 Calculating the window function. 40 nm FITC labeled beads were sparsely adsorbed onto a glass coverslip that was mounted onto to a motorized stage, and were illuminated with an arc lamp. *A*, The intensity of individual beads recorded by the APD as their image is scanned across the pinhole. *B*, The intensity of individual beads from the same sample plotted along a row of pixels in the CCD image. *C*, The average intensity profile measured by the APD in *A* (closed squares) and by the camera in *B* (closed circles) is plotted along with the average camera profile convolved by a square window function of size 3x3 (open triangles), 5.5x5.5 (open squares), and 7x7 (open diamonds) pixels.

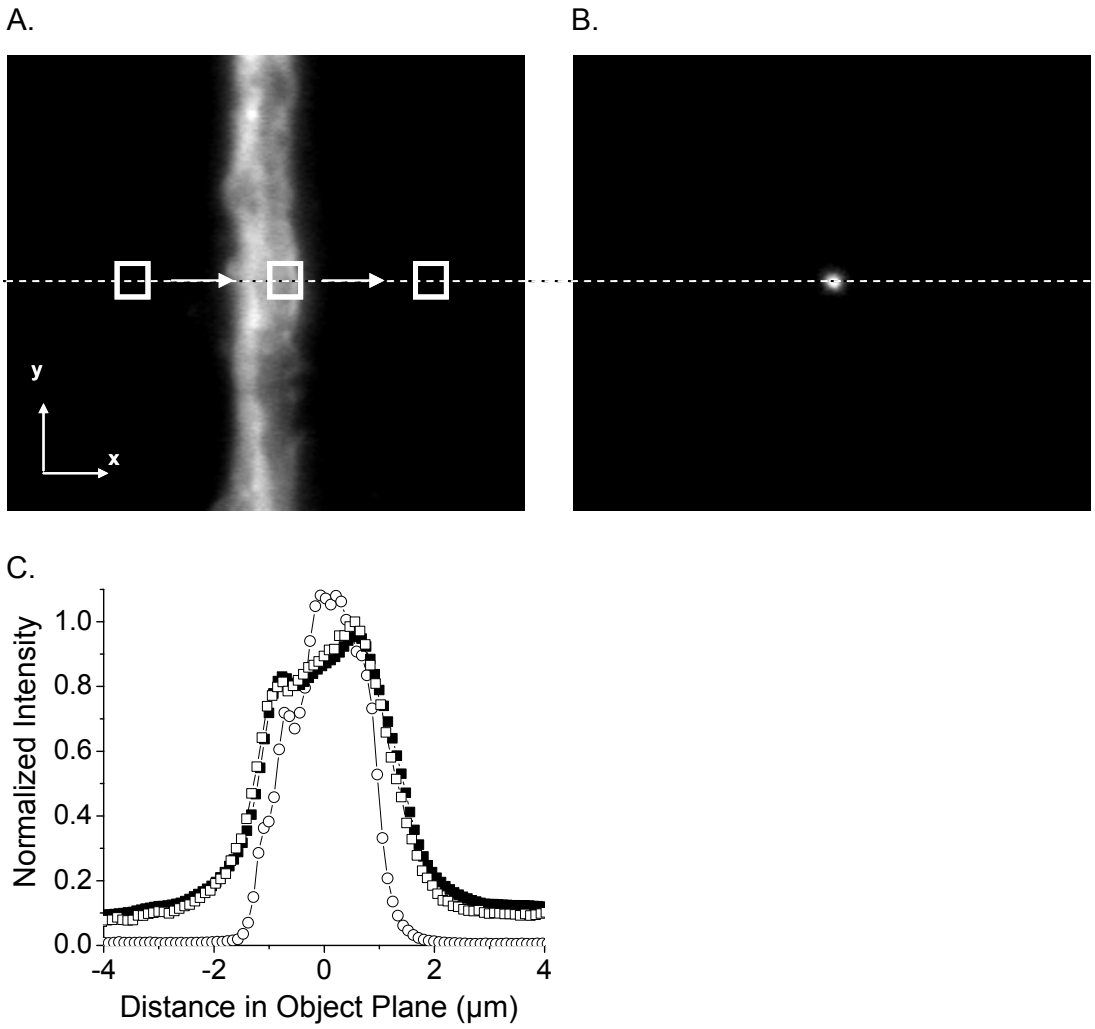

Figure 18 Counts on the CCD camera calibrated in terms of counts on the APD. *A,* A schematic of a square window function being scanned across an image of a dendrite labeled with FM 1-43 and illuminated with an arc lamp. The y coordinate for the window function is given by the position of the laser spot shown in *B. C*, This convolved intensity profile (closed squares) is scaled to the intensity profile measured by the APD as the dendrite's image is physically scanned across the pinhole (open squares). This scaling factor calibrates the counts on the 16-bit scale of the camera into photon counts measured by the APD. Notice that the two curves collapse onto each other indicating that the window function used in the convolution is accurate. The same dendrite is then illuminated with the laser spot and the image is scanned across the same pinhole and APD as above (open circles). This is scaled to best match the scan using the APD and arc lamp. This scaling factor provides the calibration of the lamp intensity in terms of the laser intensity.

B. STICK-AND-RELEASE MODEL OF VESICLE MOTION

In this and in the last appendix we describe the details underlying several of the theoretical results presented in this thesis. This work was done by Chuck Yeung, with little contribution from the author, and is included in the thesis for completeness.

In this appendix we derive the ensemble average subtracted correlation function for the stick and release model. The time average subtracted correlation function can then be obtained using the results of Appendix C.

In the stick and release model, the mobile vesicles are assumed to alternate between a state in which they are bound to the actin network (stationary) and a second state in which they are free to diffuse with a diffusion time $\tau_D=w^2/D$ where w is the width of the beam and D is the diffusion constant. They release with a rate $1/\tau_s$ when bound and bind with a rate $1/\tau_f$ when free. Here we have the changed notation used earlier in the thesis, where $\tau_s = \tau_B$ and $\tau_f = \tau_U$ to avoid confusion below. Therefore the vesicles, on average, will be bound for a time τ_s before freeing and be free for a time τ_f before binding. In steady state, the probability that a vesicle is stuck is $\tau_s/(\tau s+\tau_f)$ and free is $\tau_f/(\tau s+\tau_f)$.

The ensemble average subtracted intensity autocorrelation function is

$$G_0(t) = G_0(0)\int_0^t du\ P(u,t)\frac{1}{(1+u/\tau_D)^{d/2}}$$

where d is the dimension and $P(u,t)$ is the probability density that the vesicle is free for a total time u out of a time interval $t \geq u$. The probability density $P(u,t)$ can be obtained by summing over the probabilities of having the total free time u in total time t occurring in n different

intervals. Assuming that the vesicle is initially free, the probability density that there are *n* free and *n* stuck intervals with the total free time *u* and the total stuck time being *t-u* is

$$P^{f}_{n,n}(u,t) = \frac{1}{\tau_f (n-1)!(n-1)!}\left(\frac{u(t-u)}{\tau_f \tau_s}\right)^{n-1} e^{-(t-u)/\tau_s} e^{-u/\tau_f}, \qquad n \geq 1.$$

Assuming initially free, the probability density of having *n* free intervals and *n-1* stuck intervals is

$$P^{f}_{n,n-1}(u,t) = \frac{1}{\tau_s (n-1)!(n-2)!}\left(\frac{u}{\tau_f}\right)\left(\frac{u(t-u)}{\tau_f \tau_s}\right)^{n-2} e^{-(t-u)/\tau_s} e^{-u/\tau_f}, \qquad n \geq 2,$$

$$P^{f}_{1,0}(u,t) = e^{-t/\tau_f}\ \delta(u-t).$$

Similar expressions can be obtained assuming that the vesicle is initially stuck. Assuming initially stuck, the probability density of having *n* free and *n* stuck intervals is

$$P^{s}_{n,n}(u,t) = \frac{1}{\tau_s (n-1)!(n-1)!}\left(\frac{u(t-u)}{\tau_f \tau_s}\right)^{n-1} e^{-(t-u)/\tau_s} e^{-u/\tau_f}, \qquad n \geq 1.$$

Assuming initially stuck, the probability density of having *n* free and *n+1* stuck intervals is

$$P^{s}_{n-1,n}(u,t) = \frac{1}{\tau_f (n-1)!(n-2)!}\left(\frac{t-u}{\tau_s}\right)\left(\frac{u(t-u)}{\tau_f \tau_s}\right)^{n-2} e^{-(t-u)/\tau_s} e^{-u/\tau_f}, \qquad n \geq 2,$$

$$P^{s}_{0,1}(u,t) = e^{-t/\tau_s}\ \delta(u).$$

Multiplying the expressions above by the steady state probabilities of being free and stuck gives the probability density we need,

$$P(u,t) = \frac{\tau_f}{\tau_s + \tau_f}\sum_{n=1}^{\infty} P^{f}_{n,n}(u,t) + P^{f}_{n,n-1}(u,t) + \frac{\tau_s}{\tau_s + \tau_f}\sum_{n=1}^{\infty} P^{s}_{n,n}(u,t) + P^{s}_{n-1,n}(u,t).$$

The correlation function must be evaluated numerically and can be fairly complicated. However two limits are easy to understand. If the diffusion time τ_D is long compared to the freeing time and sticking time, then correlation function will be the same as for diffusion but with a longer effective diffusion time:

$$G_0(t) = G_0(0)\frac{1}{\left(1+(t/\tau_{D,eff})\right)^{d/2}}, \qquad \tau_D >> \tau_f, \tau_S,$$

where the effective diffusion time is:

$$\tau_{D,eff} = \frac{\tau_f + \tau_S}{\tau_f}\tau_D .$$

On the other hand, if the diffusion time is small compared to the other two time scales the sum in *P(u,t)* is dominated by the P_{10} and P_{01} terms. The correlation function is just the sum of a exponential and diffusion correlation functions

$$G_0(t) = G_0(0)\left(\frac{\tau_f}{\tau_s+\tau_f}\frac{1}{\left(1+(t/\tau_D)\right)^{d/2}} + \frac{\tau_S}{\tau_s+\tau_f}e^{-t/\tau_S}\right), \qquad \tau_D << \tau_f, \tau_S .$$

Note that in this limit, the correlation function is essentially independent of dimension for $t >> \tau_D$.

C. CORRECTION FOR FINITE INTEGRATION TIME

The intensity variations measured in most FCS experiments is the correlation of the variation of the intensity from the time average intensity for each particular experiment. On the other hand, most theoretical analysis concerns the variation of the intensity from its ensemble average value. The time average and the ensemble average intensities are the same if the integration time is much larger than the correlation time. However, this is not the case in our experiment.

In this appendix we derive the relation between the ensemble average subtracted autocorrelation function and the time average subtracted autocorrelation function. Let's introduce the notation $<x>$ and $\bar{x}$ to indicate the ensemble average and time average respectively. The ensemble average subtracted correlation function is then

$$G_0(t) = \langle \Delta I(t+s)\Delta I(s) \rangle ,$$

where $\Delta I(t) = I(t) - <I>$. We assume a steady state process so that $G_0(t)$ is independent of s. Assuming a total integration time of T, the time average intensity is

$$\bar{I} = \frac{1}{T}\int_0^T dt\ I(t) ,$$

On the other hand, the variation of the intensity from the time average intensity is

$$\overline{\Delta I}(t) = I(t) - \bar{I} = I(t) - < I > -(\bar{I} - < I >) = \Delta I(t) - \overline{\Delta I}$$

where $\overline{\Delta I} = \bar{I} - < I >$ is the difference between the ensemble average and time average intensity. Therefore the time average subtracted correlation function $G_T(t)$ can be written in terms of the ensemble average subtracted correlation function as

$$G_T(t) = \frac{1}{\Delta T}\int_0^{\Delta T} ds \left\langle \overline{\Delta I}(t+s)\,\overline{\Delta I}(s) \right\rangle = \frac{1}{\Delta T}\int_0^{\Delta T} ds \left\langle \Delta I(t+s)\,\Delta I(s) \right\rangle + \left\langle \overline{\Delta I}\ \overline{\Delta I} \right\rangle - \frac{2}{\Delta T}\int_0^{\Delta T} ds \left\langle \Delta I(s)\ \overline{\Delta I} \right\rangle$$

,

where $\Delta T=T-t$. The last two terms can be written in terms of the ensemble subtracted correlation function:

$$\left\langle \overline{\Delta I}\ \overline{\Delta I} \right\rangle = \frac{2}{T^2}\int_0^T ds \int_0^s ds'\, G_o(s')$$

and

$$\int_0^{\Delta T} ds \left\langle \Delta I(s)\ \overline{\Delta I} \right\rangle = \frac{1}{T}\int_0^{\Delta T} ds \int_0^s ds'\, G_o(s') + \frac{1}{T}\int_0^{\Delta T} ds \int_s^{T-s} ds'\, G_o(s')$$

Combining the terms gives the time average subtracted correlation function in terms of ensemble subtracted correlation function

$$G_T(t) = G_o(t) - \frac{2t}{T^2\,\Delta T}\int_0^{\Delta T} ds \int_0^s ds'\, G_o(s') - \frac{2}{T\,\Delta T}\int_0^{\Delta T} ds \int_s^{T-s} ds'\, G_o(s')$$

Notice that the time average subtracted correlation function is always smaller than the ensemble average value. If the integration time is much larger than the correlation time, the two correction terms are negligible and $G_T(t) \approx G_o(t)$. On the other hand, if the correlation time is not much smaller than the integration time, the correction terms become important and the time average subtracted correlation function can even become negative. As shown in Fig. 8B, the correction is important in our experiments even though the correlation time is less than $1/70^{th}$ of the integration time.

BIBLIOGRAPHY

Abbott, L. F. and W. G. Regehr (2004). "Synaptic Computation." Nature **431**: 796-803.

Allen, C. and C. F. Stevens (1994). "An evaluation of causes for unreliability of synaptic transmission." Proceedings of the National Acadamy of Science USA **91**: 10380-10383.

Aravanis, A. M., J. L. Pyle, et al. (2003). "Single synaptic vesicles fusing transiently and successively without loss of identity." Nature **423**: 643-647.

Benfenati, F., F. Valtorta, et al. (1991). "Computer modeling of synapsin I binding to synaptic vesicles and F-actin: Implications for regulation of neurotransmitter release." Proceedings of the National Academy of Science USA **88**: 575-579.

Berne, B. J. and R. Pecora (2000). Dynamic Light Scattering With Applications to Chemistry, Biology, and Physics. Mineola, New York, Dover Publication, Inc.

Betz, W. J. and A. W. Henkel (1994). "Okadaic Acid Disrupts Clusters of Synaptic Vesicles in Frog Motor Nerve Terminals." The Journal of Cell Biology **124**(5): 843-854.

Betz, W. J., F. Mao, et al. (1992). "Activity-dependent Fluorescent Staining and Destaining of Living Vertebrate Motor Nerve Terminals." The Journal of Neuroscience **12**(2): 363-375.

Bi, G.-q. and M.-m. Poo (1998). "Synaptic Modifications in Cultured Hippocampal Neurons: Dependence on Spike Timing, Synaptic Strength, and Postsynaptic Cell Type." The Journal of Neuroscience **18**(24): 10464-10472.

Bloch, F., W. W. Hanson, et al. (1946). "Nuclear Induction." Physical Review **69**: 127.

Burke, N. V., W. Han, et al. (1997). "Neuronal Peptide Release is Limited by Secretory Granule Mobility." Neuron **19**: 1095-1102.

Cash, S. and R. Yuste (1998). "Input Summation by Cultured Pyramidal Neurons is Linear and Position-Independent." Journal of Neuroscience **18**(1): 10-15.

Chi, P., P. Greengard, et al. (2001). "Synapsin dispersion and reclustering during synaptic activity." Nature Neuroscience **4**(12): 1187-1193.

Chi, P., P. Greengard, et al. (2003). "Synaptic Vesicle Mobilization Is Regulated by Distinct Synapsin I Phosphorylation Pathways at Different Frequencies." Neuron **38**: 69-78.

Chieregatti, E., P. E. Ceccaldi, et al. (1996). "Effects of synaptic vesicles on actin polymerization." FEBS Letters **398**: 211-216.

Colicos, M. A., B. E. Collins, et al. (2001). "Remodeling of Synaptic Actin Induced by Photoconductive Stimulation." Cell **107**: 605-616.

Coue, M., S. L. Brenner, et al. (1987). "Inhibition of actin polymerization by latrunculin A." FEBS Letters **213**(2): 316-318.

Cousin, M. A. (2005). Figure 1: The synaptic vesicle life cycle, http://www.bms.ed.ac.uk/research/idg/mbg/members/..%5Ccousin%5Cindex.htm. 2005.

Deak, F., S. Schoch, et al. (2004). "Synaptobrevin is essential for fast synaptic-vesicle endocytosis." Nature Cell Biology **6**(11): 1102-1108.

Denk, W., J. H. Strickler, et al. (1990). "Two-photon Laser Scanning Fluorescence Microscopy." Science **248**: 73-76.

Dobrunz, L. E. and C. F. Stevens (1997). "Heterogeneity of Release Probability, Facilitation, and Depletion at Central Synapses." Neuron **18**: 995-1008.

Dresbach, T., B. Qualmann, et al. (2001). "The presynaptic cytomatrix of brain synapses." Cellular and Molecular Life Sciences **58**: 94-116.

Echard, A., F. Jollivet, et al. (1998). "Interaction of a Golgi-Associated Kinesin-Like Protein with Rab6." Science **279**: 580-585.

Evans, L. L., A. J. Lee, et al. (1998). "Vesicle-associated brain myosin-V can be activated to catalyze actin-based transport." Journal of Cell Science **111**: 2055-2066.

Fernandez-Alfonso, T. and T. A. Ryan (2004). "The Kinetics of Synaptic Vesicle Pool Depletion at CNS Synaptic Terminals." Neuron **41**: 943-953.

Gennerich, A. and D. Schild (2000). "Fluorescence Correlation Spectroscopy in Small Cytosolic Compartments Depends on the Diffusion Model Used." Biophysical Journal **79**: 3294-3306.

Goda, Y. and T. C. Sudhof (1997). "Calcium regulation of neurotransmitter release: reliably unreliable?" Current Opinion in Cell Biology **9**: 513-518.

Greengard, P., F. Valtorta, et al. (1993). "Synaptic Vesicle Phosphoproteins and Regulation of Synaptic Function." Science **259**: 780-785.

Guatimosim, C., C. Hull, et al. (2002). "Okadaic acid disrupts synaptic vesicle trafficking in a ribbon-type synapse." Journal of Neurochemistry **82**: 1047-1057.

Hanse, E. and B. Gustafsson (2001). "Quantal variability at glutamatergic synapses in area CA1 of the rat neonatal hippocampus." Journal of Physiology **531**(2): 467-480.

Harata, N., J. L. Pyle, et al. (2001). "Limited numbers of recycling vesicles in small CNS nerve terminals: implications for neural signaling and vesicular cycling." TRENDS in Neurosciences **24**(11): 637-643.

Harata, N., T. A. Ryan, et al. (2001). "Visualizing recycling synaptic vesicles in hippocampal neurons by FM 1-43 photoconversion." Proceedings of the National Academy of Science USA **98**(22): 12748-12753.

Henkel, A. W., L. L. Simpson, et al. (1996). "Synaptic Vesicle Movements Monitored by Fluorescence Recovery after Photobleaching in Nerve Terminals Stained with FM 1-43." The Journal of Neuroscience **16**(12): 3960-3967.

Holt, M., A. Cooke, et al. (2004). "High Mobility of Vesicles Supports Continuous Exocytosis at a Ribbon Synapse." Current Biology **14**: 173-183.

Howard, J. (2001). Mechanics of Motor Proteins and the Cytoskeleton. Sunderland MA, Sinauer Associates, Inc.

Hume, A. N., L. M. Collinson, et al. (2001). "Rab27a Regulates the Peripheral Distribution of Melanosomes in Melanocytes." The Journal of Cell Biology **152**(4): 795-808.

Kandel, E. R. (2001). "The Molecular Biology of Memory Storage: A Dialogue Between Genes and Synapses." Science **294**: 1030-1038.

Kay, A. R., A. Alfonso, et al. (1999). "Imaging Synaptic Activity in Intact Brain and Slices with FM1-43 in C. elegans, Lamprey and Rat." Neuron **24**: 809-817.

Klingauf, J., E. T. Kavalali, et al. (1998). "Kinetics and regulation of fast endocytosis at hippocampal synapses." Nature **394**: 581-585.

Koch, C. (1999). Biophysics of Computation: Information Processing in Single Neurons. New York, Oxford University Press, Inc.

Kraszewski, K., L. Daniell, et al. (1996). "Mobility of Synaptic Vesicles in Nerve Endings Monitored by Recovery from Photobleaching of Synaptic Vesicle-Associated Fluorescence." Journal of Neuroscience **16**(19): 5905-5913.

Kricevsky, O. and G. Bonnet (2002). "Fluorescence correlation spectroscopy: the technique and its applications." Reports on Progress in Physics **65**: 251-297.

Lange, W. (1975). "Cell number and cell density in the cerebellar cortex of man and some other mammals." Cell Tissue Research **157**(1): 115-124.

Levene, M. J., J. Korlach, et al. (2003). "Zero-Mode Waveguides for Single-Molecule Analysis at High Concentrations." Science **299**: 682-686.

Liu, G. and R. W. Tsien (1995). "Properties of synaptic transmission at single hippocampal synaptic boutons." Nature **375**(6530): 404-408.

Luby-Phelps, K., P. E. Castle, et al. (1987). "Hindered diffusion of inert tracer particles in the cytoplasm of mouse 3T3 cells." Proceedings of the National Academy of Science USA **84**: 4910-4913.

Magde, D., E. Elson, et al. (1972). "Thermodynamic Fluctuations in a Reacting System - Measurement by Fluorescence Correlation Spectroscopy." Physical Review Letters **29**(11): 705-708.

Marion, J. B. and S. T. Thorton (1995). Classical Dynamics of Particles and Systems. Orlando, Harcourt Brace & Company.

Morales, M., M. A. Colicos, et al. (2000). "Actin-Dependent Regulation of Neurotransmitter Release at Central Synapses." Neuron **27**: 539-550.

Murthy, V. N., T. Schikorski, et al. (2001). "Inactivity Produces Increases in Neurotransmitter Release and Synapse Size." Neuron **32**: 673-682.

Murthy, V. N., T. J. Sejnowski, et al. (1997). "Heterogeneous Release Properties of Visualized Individual Hippocampal Synapses." Neuron **18**: 599-612.

Murthy, V. N. and C. F. Stevens (1998). "Synaptic vesicles retain their identity through the endocytic cycle." Nature **392**: 497-501.

Murthy, V. N. and C. F. Stevens (1999). "Reversal of synaptic vesicle docking at central synapses." Nature Neuroscience **2**(6): 503-507.

Neher, E. and B. Sakmann (1976). "Single-channel currents recorded from membrane of denervated frog muscle fibers." Nature **260**: 779-802.

Nielsen, E., F. Severin, et al. (1999). "Rab5 regulates motility of early endosomes on microtubules." Nature Cell Biology **1**: 376-382.

Oertner, T. G., B. L. Sabatini, et al. (2002). "Facilitation at single synapses probed with optical quantal analysis." Nature Neuroscience **6**(7): 657-664.

Ostap, M. E. (2002). "2,3-Butanedione monoxime (BDM) as a myosin inhibitor." Journal of Muscle Research and Cell Motility **23**: 305-308.

Pakkenberg, B. and H. J. G. Gundersen (1997). "Neocortical Neuron Number in Humans: Effect of Sex and Age." The Journal of Comparative Neurology **384**: 312-320.

Pakkenberg, B., D. Pelvig, et al. (2003). "Aging and the human neocortex." Experimental Gerontology **38**: 95-99.

Pieribone, V. A., O. Shupliakov, et al. (1995). "Distinct pools of synaptic vesicles in neurotransmitter release." Nature **375**(6531): 493-497.

Prekeris, R. and D. M. Terrian (1997). "Brain Myosin V Is a Synaptic Vesicle-associated Motor Protein: Evidence for a Ca2+-dependent Interaction with Synaptobrevin-Synaptophysin Complex." The Journal of Cell Biology **137**(7): 1589-1601.

Purcell, E. M., H. C. Torrey, et al. (1946). "Resonance Absorption by Nuclear Magnetic Moments in a Solid." Physical Review **69**: 37-38.

Pyle, J. L., E. T. Kavalali, et al. (2000). "Rapid Reuse of Readily Releasable Pool Vesicles at Hippocampal Synapses." Neuron **28**: 221-231.

Regehr, W. G. and C. F. Stevens (2001). Synapses. W. M. Cowan, T. C. Sudhof and C. F. Stevens. Baltimore, Johns Hopkins University Press**:** 135-175.

Rieke, F., D. Warland, et al. (1998). Spikes: Exploring the Neural Code. Cambridge, Massachusetts, MIT Press.

Rizzoli, S. O. and W. J. Betz (2004). "The Structural Organization of the Readily Releasable Pool of Synaptic Vesicles." Science **303**: 2037-2039.

Rosenmund, C. and C. F. Stevens (1996). "Definition of the Readily Releasable Pool of Vesicles at Hippocampal Synapses." Neuron **16**: 1197-1207.

Ryan, T. A. (1999). "Inhibitors of Myosin Light Chain Kinase Block Synaptic Vesicle Pool Mobilization during Action Potential Firing." The Journal of Neuroscience **19**(4): 1317-1323.

Ryan, T. A. (2001). "Presynaptic imaging techniques." Current Opinion in Neurobiology **11**: 544-549.

Ryan, T. A., H. Reuter, et al. (1997). "Optical detection of a quantal presynaptic membrane turnover." Nature **388**: 478-482.

Ryan, T. A., H. Reuter, et al. (1993). "The Kinetics of Synaptic Vesicle Recycling Measured at Single Presynaptic Boutons." Neuron **11**: 713-724.

Sankaranarayanan, S., P. P. Atluri, et al. (2003). "Actin has a molecular scaffolding, not apropulsive, role in presynaptic function." Nature Neuroscience **6**(2): 127-135.

Schikorski, T. and C. F. Stevens (1997). "Quantitative Ultrastructural Analysis of Hippocampal Excitatory Synapses." Journal of Neuroscience **17**(15): 5858-5867.

Schikorski, T. and C. F. Stevens (2001). "Morphological correlates of functionally defined synaptic vesicle populations." Nature Neuroscience **4**(4): 391-395.

Schlessinger, J., D. E. Koppel, et al. (1976). "Lateral transport on cell membranes: Mobility of concanavalin A receptors on myoblasts." Proceedings of the National Academy of Science USA **73**(7): 2409-2413.

Stevens, B. (2003). "Glia: much more than the neuron's side-kick." Current Biology **13**(12): R469-R472.

Stevens, C. F. (1994). "Cooperativity of unreliable neurons." Current Biology **4**(3): 268-269.

Stevens, C. F. and J. M. Sullivan (1998). "Regulation of the Readily Releasable Vesicle Pool by Protein Kinase C." Neuron **21**: 885-893.

Stevens, C. F. and T. Tsujimoto (1995). "Estimates for the pool size of releasable quanta at a single central synapse and for the time required to refill the pool." Proceedings of the National Academy of Science USA **92**: 846-849.

Stevens, C. F. and Y. Wang (1995). "Facilitation and Depression at Single Central Synapses." Neuron **14**: 795-802.

Stevens, C. F. and J. F. Wesseling (1998). "Activity-Dependent Modulation of the Rate at which Synaptic Vesicles Become Available to Undergo Exocytosis." Neuron **21**: 415-424.

Stevens, C. F. and J. F. Wesseling (1999). "Identification of a Novel Process Limiting the Rate of Synaptic Vesicle Cycling at Hippocampal Synapses." Neuron **24**: 1017-1028.

Stevens, C. F. and J. H. Williams (2000). ""Kiss and run" exocytosis at hippocampal synapses." Proceedings of the National Academy of Science USA **97**(23): 12828-12833.

Sudhof, T. C. (1995). "The synaptic vesicle cycle: a cascade of protein-protein interactions." Nature **375**: 645-653.

Tanaka, T., L. O. Hocker, et al. (1973). "Spectrum of light scattered from a viscoelastic gel." The Journal of Chemical Physics **59**(9): 5151-5159.

Varmus, H. (1999). "The impact of physics on biology and medicine." Physics World(September).

Wesseling, J. F. and D. C. Lo (2002). "Limit on the Role of Activity in Controlling the Release-Ready Supply of Synaptic Vesicles." Journal of Neuroscience **22**(22): 9708-9720.

Yarrow, J. C., T. Lechler, et al. (2003). "Rapid de-localization of actin leading edge components with BDM treatment." BMC Cell Biology **4**(5).